Chemical kinetic modeling of diethoxymethane oxidation

Li, Runzhao; Herreros, Martin; Tsolakis, Athanasios; Yang, W

DOI:
10.1016/j.fuel.2021.120217

Document Version
Peer reviewed version

Citation for published version (Harvard):
Li, R, Herreros, M, Tsolakis, A & Yang, W 2021, 'Chemical kinetic modeling of diethoxymethane oxidation: a carbon–neutral fuel', *Fuel*, vol. 291, 120217. https://doi.org/10.1016/j.fuel.2021.120217

Chemical kinetic modeling of diethoxymethane oxidation: A carbon-neutral fuel

Runzhao Li,[†] Jose Martin Herreros,[†] Athanasios Tsolakis,[*,†] Wenzhao Yang [‡]

[†] *Department of Mechanical Engineering, School of Engineering, College of Engineering and Physical Sciences, University of Birmingham, Edgbaston, Birmingham B15 2TT, United Kingdom*

[‡] *Shenzhen Gas Corporation Ltd., No.268, Meiao 1st Road, Futian District, Shenzhen 518049, China*

Abstract

Diethoxymethane (DEM) is a carbon-neutral fuel with high cetane number (57.3). A detailed chemical kinetic mechanism for DEM oxidation covering low and high temperature reactions is first developed in this work. The reaction scheme and rate rules of DEM sub-mechanism are determined by the analogy method to n-heptane. Aramco 3.0 mechanism is used as a base mechanism to consider C0-C4 fuels while dimethoxymethane mechanism is included to ensure the mechanism compatibility and rate rule consistency. Thermodynamic and transport properties of new species in DEM sub-mechanism are computed by the methods of group additivity and properties correlation. The mechanism is validated against ignition delay times and premixed laminar flame speed measured by shock tube, rapid compression machine and spherical flame in combustion vessel. The verification covers a pressure range of 2~30bar, an equivalence ratio range of 0.5~2.0, a temperature range of 540~1371K. A satisfactory agreement between the experimental and computed results is observed, supporting the proposed reaction

[*]Corresponding author.

E-mail address: a.tsolakis@bham.ac.uk (A. Tsolakis)

scheme and rate rules. Comparison of the ignition delay times between DEM and n-heptane indicates: (i) DEM is more reactive at low temperature (500~670K) than n-heptane which favors low temperature combustion mode. (ii) DEM ignition delay times demonstrate monotonous temperature dependence at the full temperature regime but it is relatively independent of temperature at intermediate temperature (620~960K). Therefore, a negative temperature coefficient (NTC) behavior is not observed in most conditions. (iii) DEM may not be an efficient chemical ignition source compared to n-heptane due to insufficient temperature increases and active radical accumulation.

Highlights:

- A detailed chemical kinetic mechanism for DEM oxidation is developed.
- Current mechanism includes the low and high temperature reactions to extend application domain.
- Current mechanism is validated against ignition delay times and laminar flame speeds.
- DEM is more reactive at low temperature than n-heptane favoring advanced combustion modes.
- DEM ignition delay time decreases with increasing temperature and NTC behavior is weak.

Keywords:

Carbon neutral fuels; Diethoxymethane oxidation; Mechanism development; Chemical kinetics; Fuel reactivity.

Nomenclature

Symbols

P_{init}	mixture initial pressure (used to describe boundary conditions)
T_{init}	mixture initial temperature (used to describe boundary conditions)

Greek letters

φ	equivalence ratio

Abbreviations

BECCS	bioenergy with carbon capture and storage
CaL	calcium carbonate looping
CCS	carbon capture and storage
CLC	chemical looping combustion
CFD	computational fluid dynamics
CN	cetane number
DAC	direct air capture
DEM	diethoxymethane
DMM	dimethoxymethane
EOR	CO2-enhanced oil recovery
FSC	Fuel Science Center

GHG	green house gas
HTHR	high temperature heat release
LTC	low-temperature combustion
LTHR	low-temperature heat release
NTC	negative temperature coefficient
P2X	Power-to-X
PODE	Polyoxymethylene Dimethyl Ether
RCM	rapid compression machine
SCU	Sichuan University
SFN	Solar Fuels Network
ST	shock tube
UCL	Université catholique de Louvain
UOB	University of Birmingham

39

1. INTRODUCTION

European Union commits to cut greenhouse gas (GHG) emissions by 80~95% after 2050 to prevent a global average temperature increase above 2°C within the 2015 Paris Agreement. Replacing fossil fuels with carbon-neutral fuels could close the carbon cycle and reach zero net CO_2 emission. The carbon-neutral fuels produced in the sustainable carbon cycle are shown in Fig. 1 and the synthetic gas ($CO+H_2$) is the key platform chemicals. The CO or carbon atom is supplied by carbon capture and storage (CCS) technology. The CO_2 is collected and condensed from non-edible biomass, ambient and thermal power plant emission. The commercial-scale or demonstration-scale CO_2 capture technologies include chemical absorption using aqueous amine solutions, polymeric membranes, bioenergy with carbon capture and storage (BECCS), post-combustion adsorption, oxy-combustion coal power plant, direct air capture (DAC). Chemical looping combustion (CLC) and calcium carbonate looping (CaL) technologies are still conducted in pilot-scale operation [1]. The CO_2 transportation technologies are well established through worldwide on-shore & off-shore pipelines and transport ships [1]. The commercial scale or demonstration-scale CO_2 storage technologies include saline formation, CO_2-enhanced oil recovery (EOR), depleted oil & gas fields while ocean storage and mineral storage are still in formulation and lab test phases [1]. Afterward, the CO_2 is processed and transformed through thermo-catalytic routes and electrochemical routes to produce CO, O_2, CH_4 as shown in Fig. 1. H_2 is generated by water splitting through electrochemical routes and the power source is supplied by renewable energy such as wind and solar electricity. Ethers, alcohols and hydrocarbons can be produced from synthetic gas through Fischer-Trosch synthesis under different types of catalysts [2]. These sustainable ethers, alcohols and hydrocarbons used in the combustion process of transportation and industrial power generation sectors can achieve zero net emission of CO_2. As a result, the concept of carbon-neutral fuel receives increasing

attention evidenced by the mainstream research projects including but not limited to:

1. ENERGY-X project (European Commission): This Horizon 2020 project aims to address the efficient conversion from solar/wind energy to chemicals [2].
2. SUNENERGY project (European Commission): It builds on two Horizon 2020 projects of SUNRISE and ENERGY-X. It aims at using renewable energy from sunlight/wind and abundant molecules of CO_2/H_2O/N_2 to produce fossil-free fuels and chemicals [3].
3. Solar Fuels Network (UK, SFN): It aims at using sunlight to electrolyze water into H_2 coupling CO_2 to make fuels [4]. The carbon-neutral fuels are manufactured by solar-driven fuel synthesis.
4. Power-to-X (European Commission): Based on the prerequisite of full decarbonization of the power sector by 2050, appropriate energy carriers are required to store the sustainable electricity. It evaluates the potential and competitiveness of 3 major power-to-X technologies (including power-to-H_2, power-to-CH_4 and power-to-liquid fuels) as the energy carrier of sustainable electricity by 2050. [5]
5. Kopernikus project-P2X (Germany): The goal is to store renewable energy in a physical substance that converts renewable electricity (produced by solar, wind, and hydropower) into chemical energy. This chemical energy can be used in the transportation sector, industry sector or even high-emission sector but still environmentally friendly. It tries to partially or replace fossil diesel/gasoline/aviation fuels with synthetic fuels derived from syngas [6, 7].
6. The Fuel Science Center (Germany): It integrates renewable electricity and bio-based carbon feedstock/CO_2 to supply high-density liquid energy carriers termed as “bio-hybrid fuels” [8, 9]. It aims at reducing the carbon footprint significantly by these tailor-made bio-hybrid fuels.
7. Co-Optimization of Fuels & Engines: It intends to improve the fuel economy and emission

84 performance by co-optimization of fuels and engines. One of the fuel screening criteria for both
85 SI and CI engines is that the candidates can be produced from renewable domestic biomass as
86 replacements for fossil fuels [10-12].

87 Table 1 summarizes the typical n-alkanes and ethers which can be synthesized through the Fischer-
88 Trosch process. The fuel molecules located in the same column have the same total number of C-atoms
89 and O-atoms while those in a single row have an identical number of O-atoms. Those fuel compounds
90 with reference indicate that the comprehensive mechanisms covering low and high temperatures
91 reactions are available. Diethoxymethane (DEM) has a cetane number (CN) of 57.3 [13] which can be
92 synthesized by ethanol, H_2 and CO_2 using Ruthenium catalyst [14]. There are only two DEM high
93 temperature oxidation mechanisms available in the literature: one is proposed by Dias et al. [15, 16]
94 which is also known as UCL (Université catholique de Louvain) mechanism. It describes the flat flame
95 stabilized at low pressure of 50mbar and it may encounter convergence problem when running at engine
96 relevant pressure. The other is proposed by Zhang et al. [17] and it is referred to SCU (Sichuan University)
97 mechanism in this work. It testes the ignition delay times at φ=0.5, 1.0, 2.0, T_{init}= 1065~1370 K, P_{init}= 2,
98 4, 10 atm using shock tube. However, there are fundamental knowledge gaps in both mechanisms: First,
99 both mechanisms contain only high temperature reactions but lack low temperature reactions, thus they
100 cannot reproduce the ignition phenomenon occurred at low and intermediate temperature (500~1000K)
101 regimes. Second, the UCL mechanism applies only to low pressure since the impact of pressure is not
102 considered in the pressure dependent reactions. Third, the rate constants of elementary reactions used in
103 those mechanisms are not up to date which has been developed 5~10 years ago. Recently, rate constants
104 for the reactions of H-atom abstraction from DEM by H, CH_3, C_2H_5 and the followed β-scission reactions
105 are computed by Kröger et al. [18] using high-level CCSD(T)/aug-ccpV(T+D)Z//B2PLYPD3BJ/6-

311++(d,p) theory and transition state theory. The experimental DEM ignition delay times covering the full temperature range (590~1090K) measured in shock tube (ST) and rapid compression machine (RCM) have been reported by Lehrheuer et al. [19]. The premixed laminar flame speeds at 1.01, 2.50 bar are measured in a spherical flame by Kopp et al. [20]. These data provide the foundation to develop the full-scale DEM oxidation mechanism.

Detailed chemical kinetic mechanisms are required to mimic the conventional and alternative fuels combustion process in devices (industrial burners, gas turbines, boilers, incinerators, gasifiers, internal combustion engines, etc.) and formulate the fuel compositions. Detail mechanism contains reaction rate constant of elementary reactions, species thermodynamic/transport parameters and reaction pathway. It tries to incorporate all the necessary species and reactions to reproduce the experimental results [21]. Rate constants need to be assigned to a large number of elementary reactions in the detailed mechanism, thus, elementary reactions are assigned to various reaction classes with associated reaction rate rules [22, 23]. The detailed mechanism assembles the species, reactions with specified rate constants and validates against experimental data from fundamental combustion devices (e.g. shock tube, rapid compression machine, flame burner, jet stirred reactor, flow reactor). Coupling detailed mechanism with computational fluid dynamics (CFD) to study the combustion phenomena demands substantial computing sources, therefore, several mechanism reduction technologies (skeletal reduction, chemical species lumping, time-scale analysis, stiffness reduction and on-the-fly reduction) can be applied to obtain reduced mechanism [24].

A detailed chemical kinetic mechanism for DEM oxidation over the low, intermediate and high temperature regimes is first reported in this work. The latest Aramco 3.0 mechanism is employed as a base mechanism while the dimethoxymethane (DMM) mechanism is adopted to improve the mechanism

128 compatibility and connect the base mechanism and DEM sub-mechanism. The proposed mechanism is
129 validated against the observed ignition delay times and laminar flame speed. The ignition delay times
130 between DEM and n-heptane are compared under a wide range of conditions to reveal the fuel oxidation
131 characteristics.

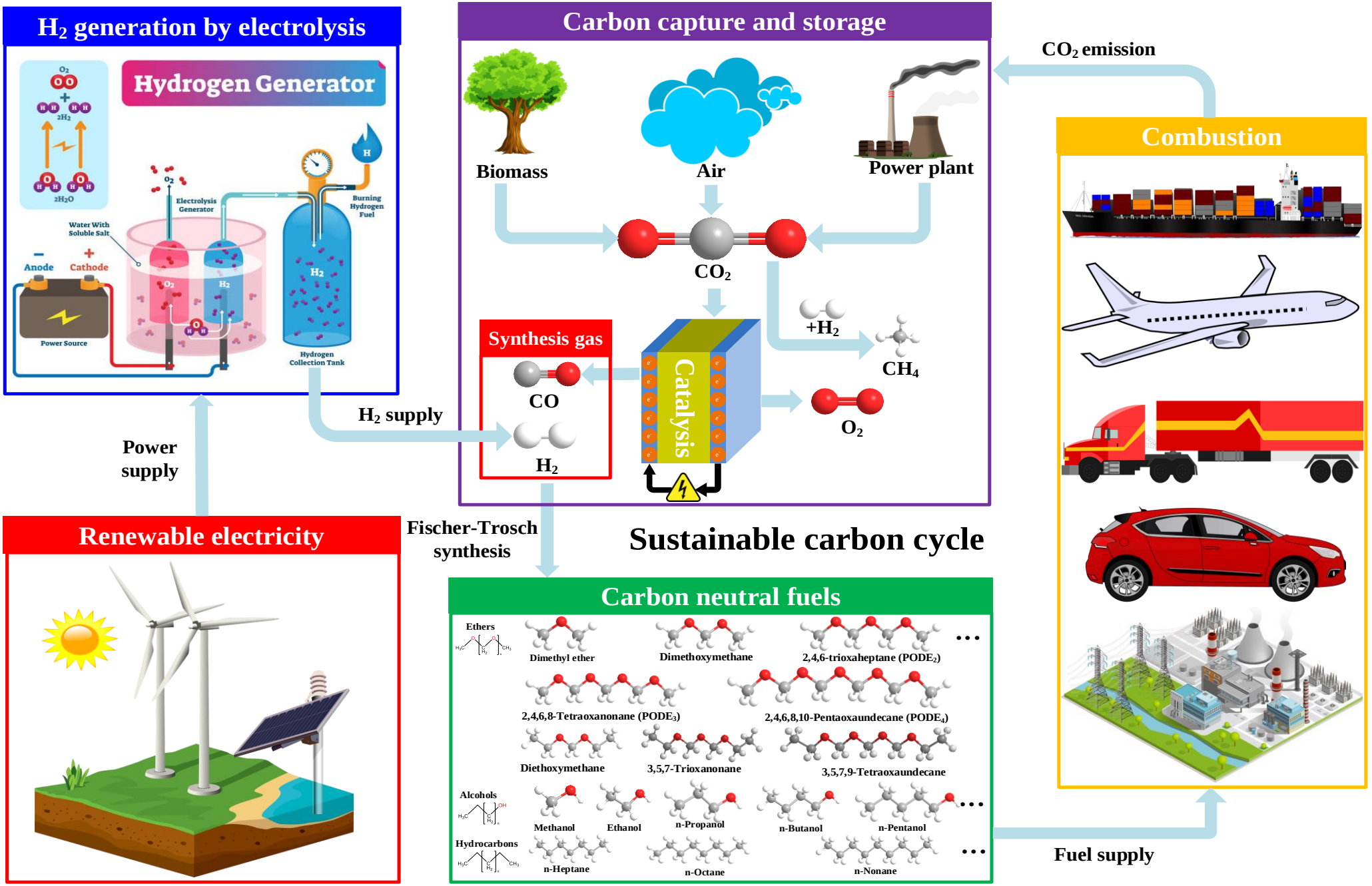

Fig. 1. Carbon neutral fuels produced in a sustainable carbon cycle.

Table 1. Overview of C3, C5, C7, C9, C11 alkanes and corresponding ethers with 1~5 O-atom substituents.

No.	3[α]	5	7	9	11
0[β]	n-Propane [25-27][γ] 	n-Pentane [26-29] 	n-Heptane [23, 30, 31] 	n-Nonane [31] 	n-Undecane [31] 
1	Dimethyl ether [32] 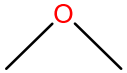	Diethyl ether [33, 34] 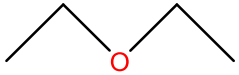	Dipropyl ether [35] 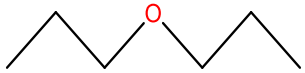	Dibutyl ether [36, 37] 	Dipentyl ether 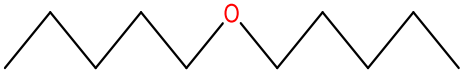
2	N/A	Dimethoxymethane [32, 38, 39] 	Diethoxymethane, this work 	Dipropoxymethane 	Dibutoxymethane 
3	N/A	N/A	2,4,6-trioxaheptane (PODE2) [40] 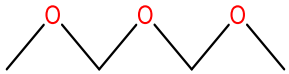	3,5,7-Trioxanonane  2,5,8-Trioxanonane 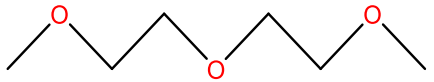	Propoxymethyl ether 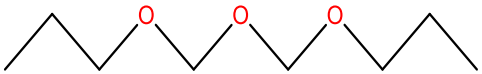 3,6,9-Trioxaundecane 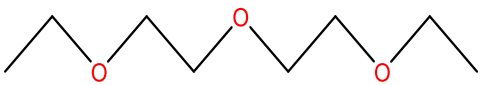 2,6,10-Trioxaundecane 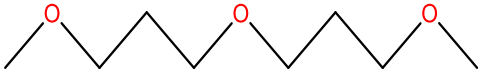
4	N/A	N/A	N/A	2,4,6,8-Tetraoxanonane (PODE3) [40-43] 	3,5,7,9-Tetraoxaundecane  2,5,7,10-Tetraoxaundecane 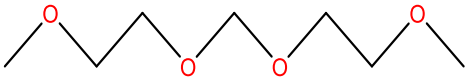
5	N/A	N/A	N/A	N/A	2,4,6,8,10-Pentaoxaundecane (PODE4) [40] 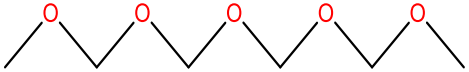

[α] Number in the first row is the total number of C-atoms and O-atoms;

[β] Number in the first column is the total number of O-atoms.

γ The newly-published comprehensive mechanisms covering low and high temperature reactions are provided in the reference and those without reference denote comprehensive mechanisms are unavailable so far.

2. CHEMICAL KINETIC MECHANISM FORMULATION

2.1 Mechanism development and naming of species

The physicochemical properties of DEM are listed in Table 2. Two sets of detailed DEM oxidation mechanisms have been developed, one covering low and high temperature reactions (735 species, 3488 reactions) and the other containing high temperature reactions only (333 species, 1661 reactions). Both low-high temperature and high temperature version UOB (University of Birmingham) mechanisms (chemical kinetic mechanisms, thermodynamic parameters and transport parameters) are available in the Supplementary Material and the Data in Brief. The DEM low-high temperature mechanism is specially developed to model gas-phase combustion process (e.g. ignition-delay times, steady-state gas-phase combustion, temperature and species evolution in autoignition process) which composes of Aramco 3.0 sub-mechanism [44], dimethoxymethane (DMM) sub-mechanism [38] and DEM sub-mechanism. Aramco 3.0 sub-mechanism describes the oxidation process of C_0-C_4 fuels (H_2, CO, methane, ethane, ethylene, acetylene, formaldehyde, acetaldehyde, propane, butane, etc.), C_5-C_7 normal paraffin and their isomers (n-pentane, iso-pentane, neo-pentane, n-hexane), monoaromatics (benzene, phenol, cyclopentadiene, fulvene, etc.), PAHs (indene, naphthalene, fluprene etc.), C_1-C_3 alcohols (methanol, ethanol, n-propanol, iso-propanol etc.) as shown in Fig. 2. DMM mechanism proposed by Javob et al. [38] is adopted to connect the Aramco 3.0 [44] and DEM sub-mechanism developed in this work. This DMM mechanism uses Aramco 2.0 [45] as a base mechanism which ensures the overall compatibility of Aramco 3.0 [44], DMM and DEM sub-mechanism.

The DEM high temperature oxidation mechanism is specifically developed for flame modeling (e.g. laminar flame speed, burner-stabilized flame, opposed-flow flame, flame extinction analysis, stagnation flame analysis, etc.) which comprises of $PODE_{2-4}$ base mechanism [38] and diethoxymethane sub-mechanism. $PODE_{2-4}$ mechanism [38] is employed to describe the reactions of C_0-C_4 small molecules which commonly appearing in

161 the oxidation of the large hydrocarbon. Meanwhile, this mechanism also incorporates DMM sub-mechanism. The
162 role of the $PODE_{2-4}$ base mechanism [38] in DEM high temperature oxidation mechanism plays the same role as
163 Aramco 3.0 [44] and DMM [38] mechanisms in DEM low-high temperature oxidation mechanism. But the
164 $PODE_{2-4}$ base mechanism [38] mainly focuses on the high temperature oxidation process and thus the mechanism
165 size is much smaller than Aramco 3.0 [44] and DMM [38] mechanisms.

166 DEM and n-heptane have similar molecular structures such as straight-chain and symmetric structures as shown
167 in Fig. 3. Replacing two C-atoms at position 3 in n-heptane molecule with O-atoms becomes DEM molecule. The
168 analogy method can be implemented to design the reaction scheme and estimate the rate constants of elementary
169 reactions for DEM sub-mechanism due to their similar molecular structure. C_7H_{15}_1, C_7H_{15}_2, C_7H_{15}_3, C_7H_{15}_4
170 are the four products of H-atom abstraction from n-heptane [23, 30]. O-atoms occupy position 3 for DEM, thus
171 there are 3 H-atom abstraction pathways at positions 1, 2, 4. They are C2H4OCH2OC2H5 (DEM1),
172 CH3CHOCH2OCH2CH3 (DEM2) and CH3CH2OCHOCH2CH (DEM3) respectively [15, 16] [17]. The
173 represented species in DEM mechanism and the analogical species in the n-heptane mechanism are presented in
174 Table 3. The full species glossary for DEM sub-mechanism is provided in supporting information.

175 The similar molecular structures between DEM and n-heptane result in a similar oxidation pathway as shown
176 in Fig. 4. Low temperature (T_{init}=500~625K) oxidation initiates with H-atom abstraction from DEM to form
177 DEMx (DEM1, DEM2 DEM3). The first O_2 addition to DEMx to form $DEMxO_2$ (including $DEM1O_2$, $DEM2O_2$,
178 $DEM3O_2$) and then $DEMxO_2$ isomerizes to produce QOOH. The second O_2 addition takes place on QOOH to
179 produce O2QOOH. 1st O2 addition, QOOH isomerization and 2nd O_2 addition are the typical reactions for DEM
180 low temperature oxidation. QOOH takes place low temperature degenerated branched chain reaction to produce
181 carbonylhydroperoxide and OH radical. The carbonylhydroperoxide further decomposes to form oxygenated and
182 OH radicals by chain branching reactions. EROOH is the isomerized product of O2QOOH and low temperature

chain branching reaction takes place to produce ERO and OH radical. QOOH decomposition occurs at the mediate temperature (T_{init}=625~900K) through three pathways: (1) QOOH<=>cyclic ether+OH; (2) QOOH<=>ether with carbon double bond+HO2; (3) QOOH<=>β-scission products. At high temperature regime (T_{init}>900K), DEM comes across carbon-oxygen bond cleavage to form active radicals while the n-heptane takes place carbon-carbon bond cleavage.

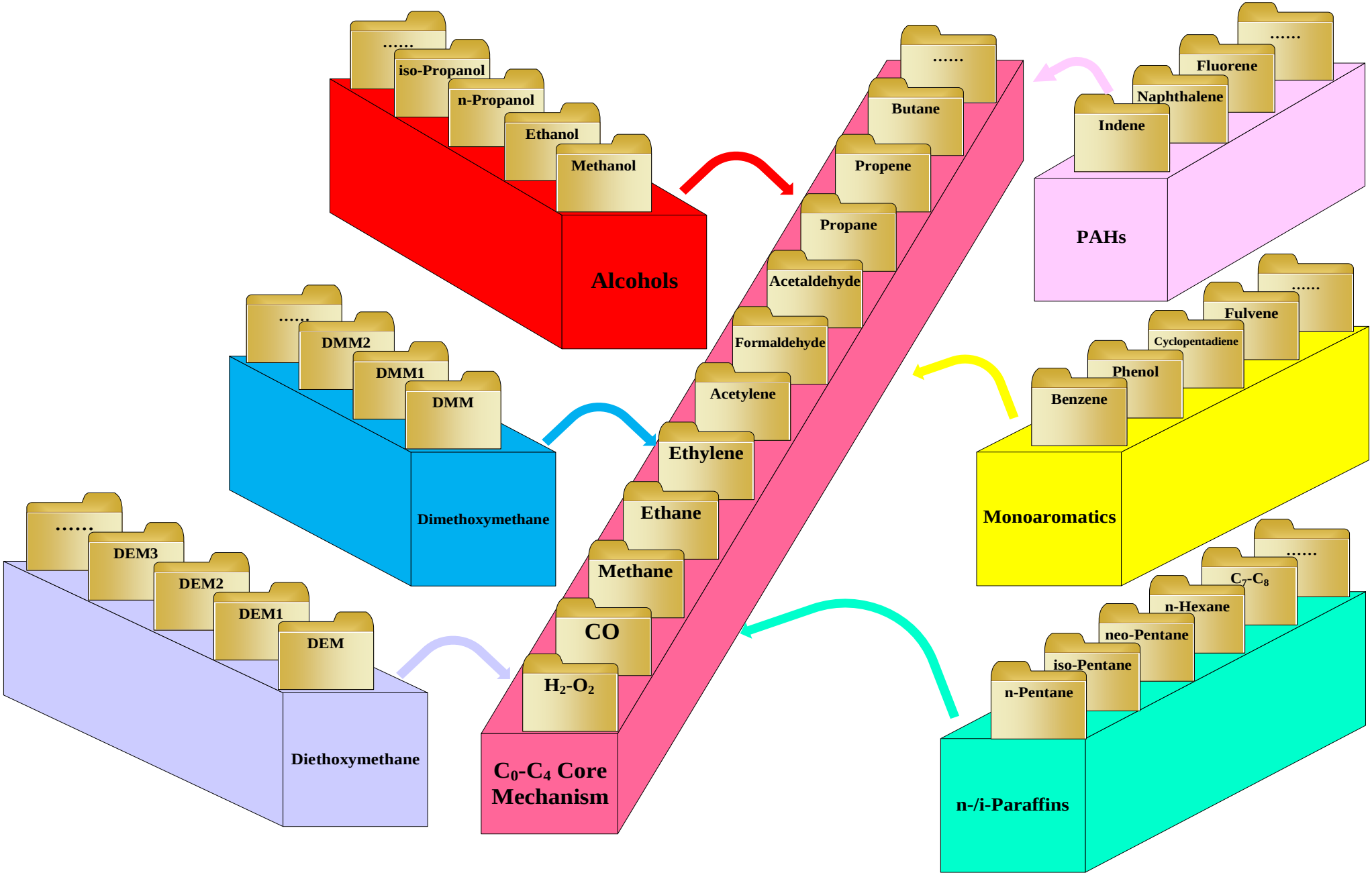

Fig. 2. The hierarchical/modular structure and overall interrelationships between component libraries in the detailed DEM mechanism.

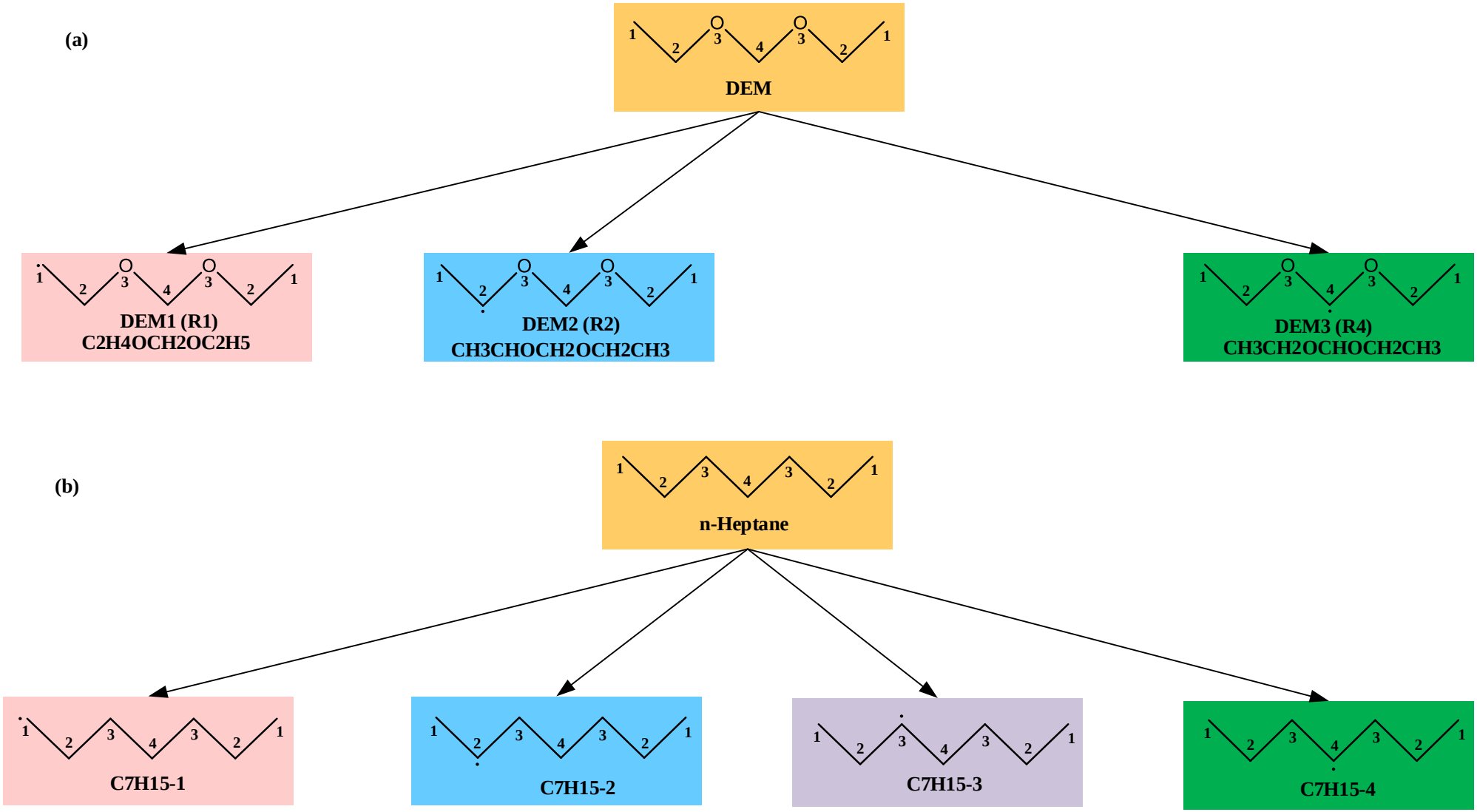

Fig. 3. Molecular structure of (a) DEM, (b) n-heptane and major products by H-atom abstraction from fuel.

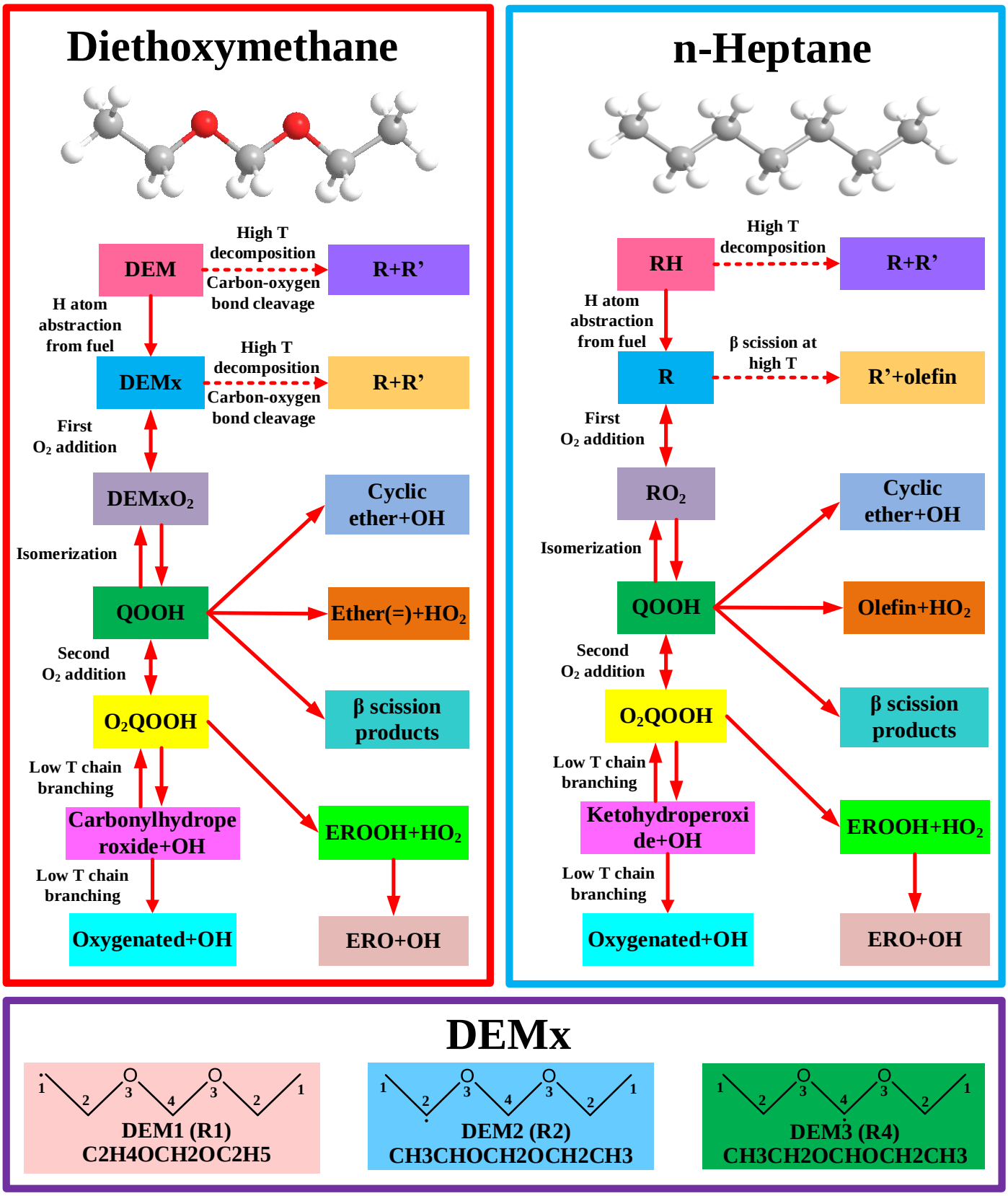

Fig. 4. Comparison of major oxidation pathways between DEM and n-heptane [30].

194 **Table 2.** Physicochemical properties of DEM.

Name	Diethoxymethane or Ethylal
CAS	462-95-3
Formula	C5H12O2
Molecular structure	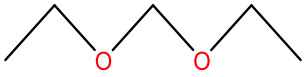
Molecular weight	104.15
Boiling point (ºC)	88.05 [46]
Melting Point (ºC)	-66.5 [47]
Flash point (ºC)	-5 [48]
Enthalpy of vaporization (kJ/mol)	35.74 [46]
Cetane number	57.3 [13]
Lower heating value (MJ/kg)	29.7 [19]

195

196 **Table 3.** Represented species in DEM mechanism and analogy species in n-heptane mechanism [30].

Name (DEM)	Molecular structure	Name (n-heptanne)	Molecular structure
DEM		nC7H16	
DEM2/ CH3CHOCH2OCH2CH3		C7H15-2	
DEM2O2/ CH3COOHOCH2OC2H5	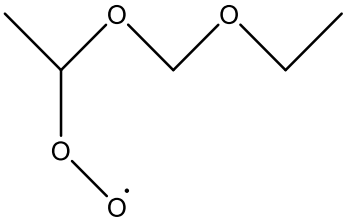	C7H15-2O2	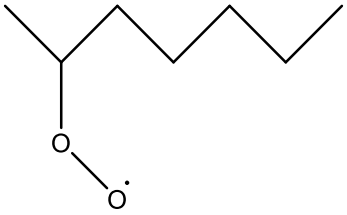
C2H5OCH2OCHCH2		C7H14-1	
C2H5OCOCOOHHCH3	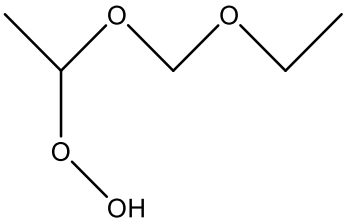	C7H15OOH-2	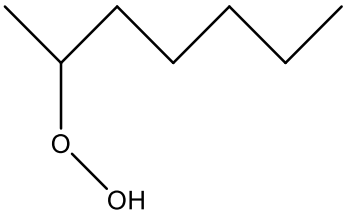
C2H5OCOCOHCH3	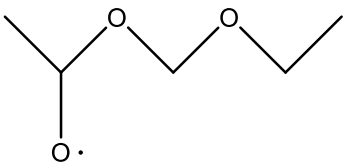	C7H15-2O	
CH3CHOCOCOOHHCH3	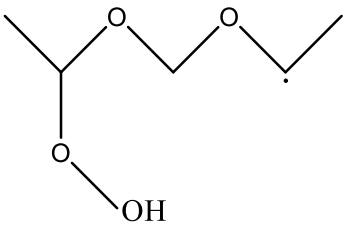	C7H14OOH2-6	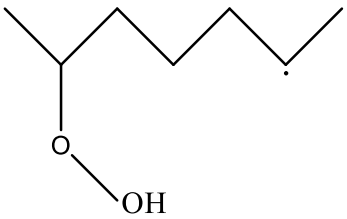
CH3COOOCOCOOHCH3	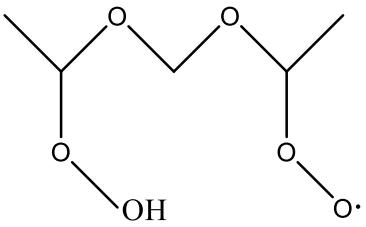	C7H14OOH2-5O2	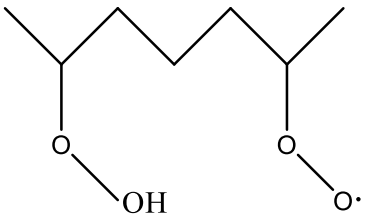
CH3COOCOCOOHHCH3	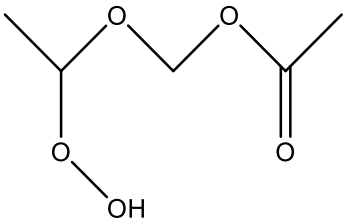	C7KET26	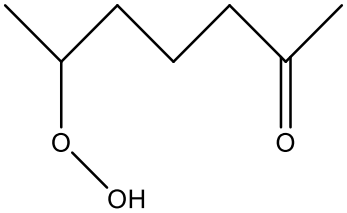
CH3COOCOCOHCH3	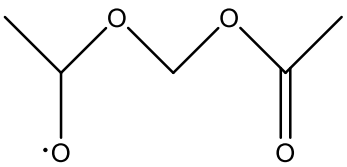	C7KET26O	

197

198 **2.2 Classes of reactions**

199 Reaction classes generalize the kinetic information of reaction pathways and rate constants that
200 systematically embody the analogies and physical principles. They essentially describe: (1) when the
201 reaction classes should be applied within particular chemical reactants; (2) how the specific reactants
202 transform to products through a series of elementary reactions; (3) the rate constants associated with the
203 conversion from reactants to products [21]. There are 13 high temperature reaction classes and 24 low
204 temperature reaction classes considered in the current DEM oxidation mechanism as shown in Table 4
205 and Table 5 respectively. The rate constants of elementary reactions from the Aramco 3.0 base
206 mechanism [44] and DMM sub-mechanism [38] remain unchanged. For the DEM sub-mechanism, the
207 elementary reactions from high temperature reaction classes derive from the UCL mechanism [15, 16]
208 and SCU mechanism [17] respectively. Those reactions belong to low temperature reaction classes
209 mainly refer to the n-heptane oxidation mechanism [30] according to the analogy method.

210 The DEM low temperature oxidation reaction pathways have been discussed in the last paragraph of
211 section 2.1 and the major reaction routes are presented in Fig. 5. The full reaction pathway is provided
212 in Fig. S1 of supporting information in Supplementary Material. The major difference between DEM and
213 n-heptane is the low temperature oxidation reactivity, thus the ignition delay time of DEM is lower by
214 an order of magnitude than n-heptane at T_{init}=500~650K [49]. Therefore, both pre-exponential factor A,
215 temperature exponents n of reaction class 3 (H-atom abstraction from fuel, initiation reactions) in DEM
216 mechanism increase compared to n-heptane to elevate low temperature reactivity. Their rate constants
217 are compared in Fig. 6 and the pre-exponential factor A, temperature exponents n and the activation
218 energy E_a are listed in Table 6. The H-atom abstraction from DEM by C_2H_5 radical is first introduced in
219 the DEM oxidation mechanism which is not included in the SCU mechanism [17] and UCL mechanism

220 [15, 16]. C_2H_5 radical is DEM β-scission products through Eq. (1) ~ Eq. (2) (belong to reaction class 1),
221 thence this radical play a non-negligible role in DEM low temperature ignition. DEM1, DEM2, DEM3
222 occur the 1st O_2 addition to produce $DEM1O_2$, $DEM2O_2$, $DEM3O_2$ through Eq. (3) ~ Eq. (5). $DEM1O_2$,
223 $DEM2O_2$, $DEM3O_2$ undergo isomerization by internal H-atom transfer to form QOOH. 5 to 10 member
224 ring is the intermediate transition state structure during the isomerization reaction as shown in Fig. 7.
225 QOOH radicals take place 2nd O_2 addition to produce O_2QOOH which decomposes into
226 carbonylhydroperoxide and OH radicals as shown in Fig. 5. Carbonylhydroperoxide further decomposes
227 to produce oxygenated radicals and OH radicals. These two steps constitute the degenerate chain
228 branching reactions for DEM low temperature oxidation. Reaction class 1 and 4, for example Eq. (6) and
229 Eq. (7), also play a key role to reduce the fuel reactivity at low and intermediate temperature regime
230 (ranges from 500K to 960K) in addition to reaction class 3.

231 DEM<=>C2H5OH+C2H5+HCO (1)

232 DEM<=>C2H5OCH2O+C2H5 (2)

233 C2H4OCH2OC2H5+O2<=>C2H5OCH2OC2H4OO (3)

234 CH3CHOCH2OCH2CH3+O2<=>CH3COOHOCH2OC2H5 (4)

235 CH3CH2OCHOCH2CH3+O2<=>C2H5OCOOHOC2H5 (5)

236 DEM<=>CH2OCH2OC2H5+CH3 (6)

237 CH2OCH2OC2H5<=>C2H5OCH2+CH2O (7)

238

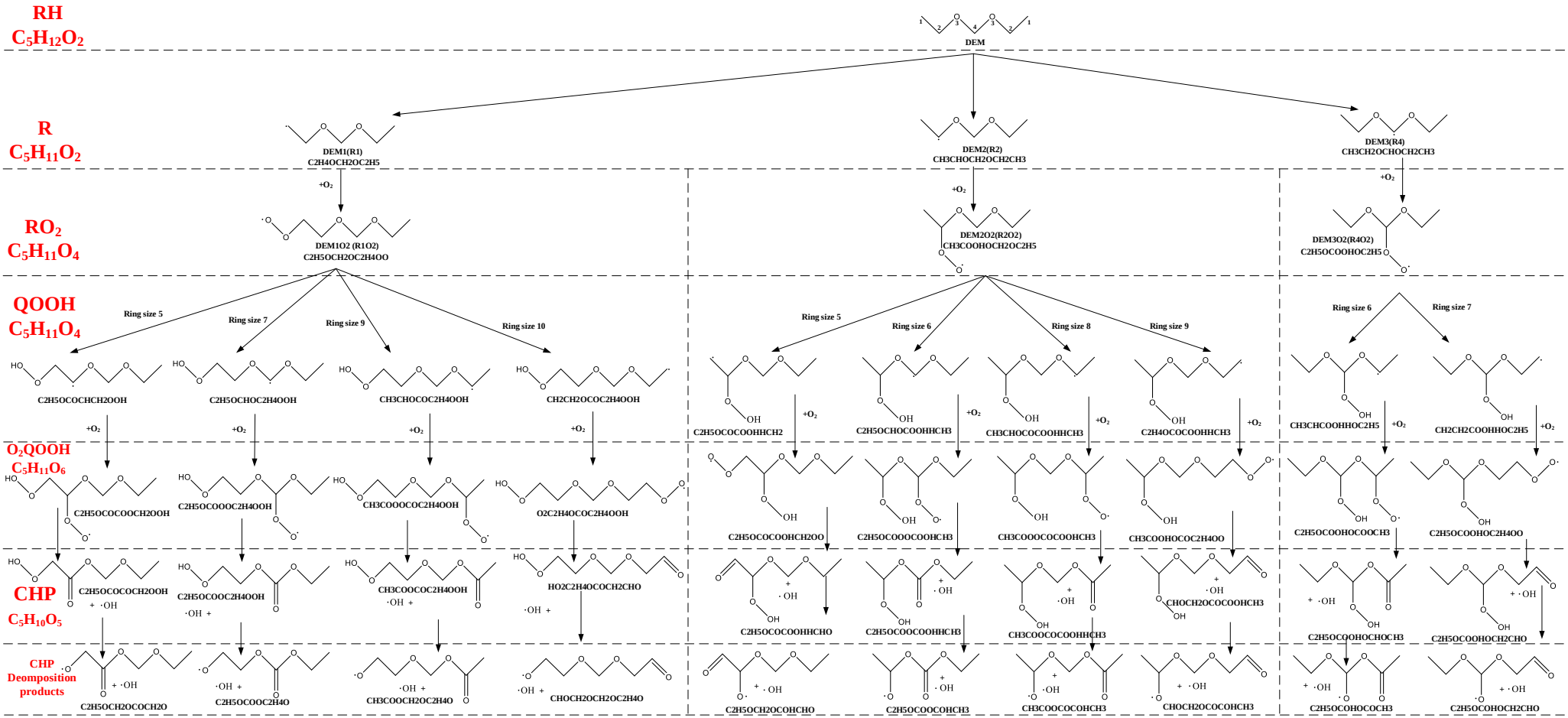

Fig. 5. Proposed key DEM low temperature oxidation reaction pathways and the full pathway is provided in supporting information.

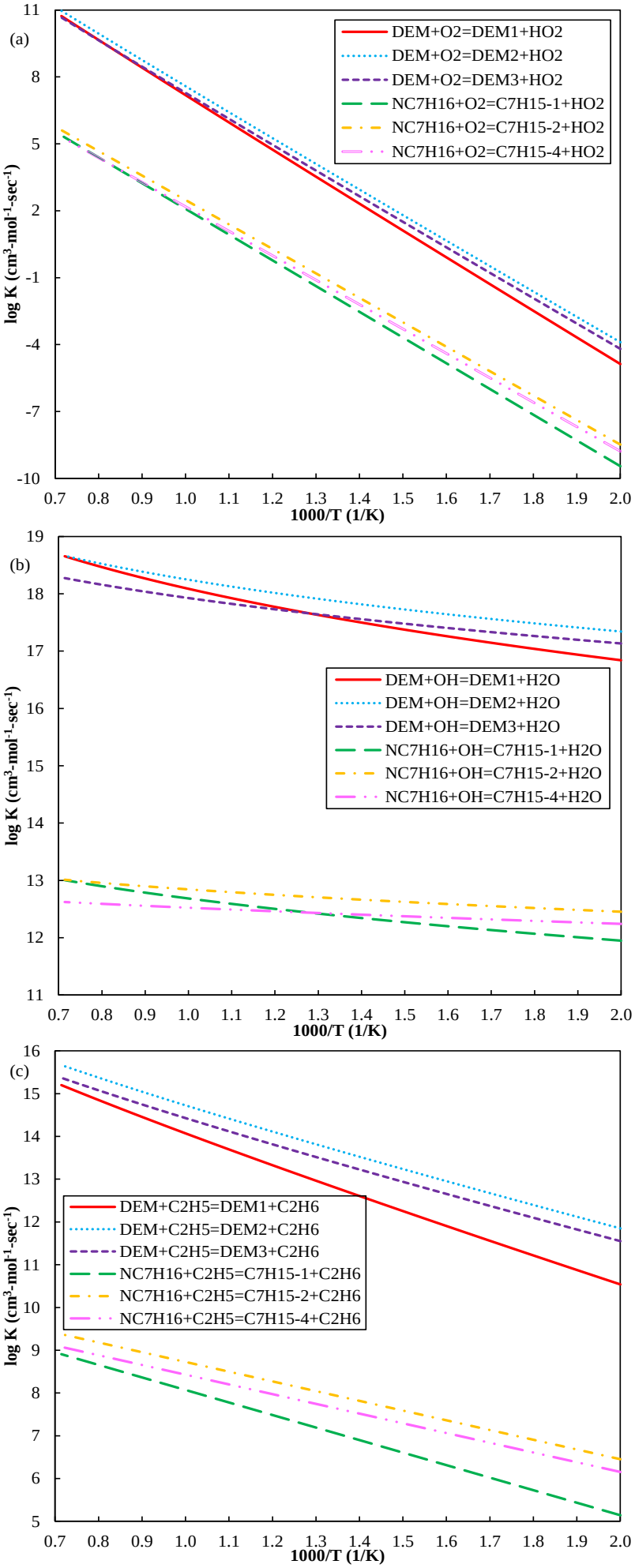

Fig. 6. Rate constants of H atom abstraction reactions for diethoxymethane and n-heptane [30].

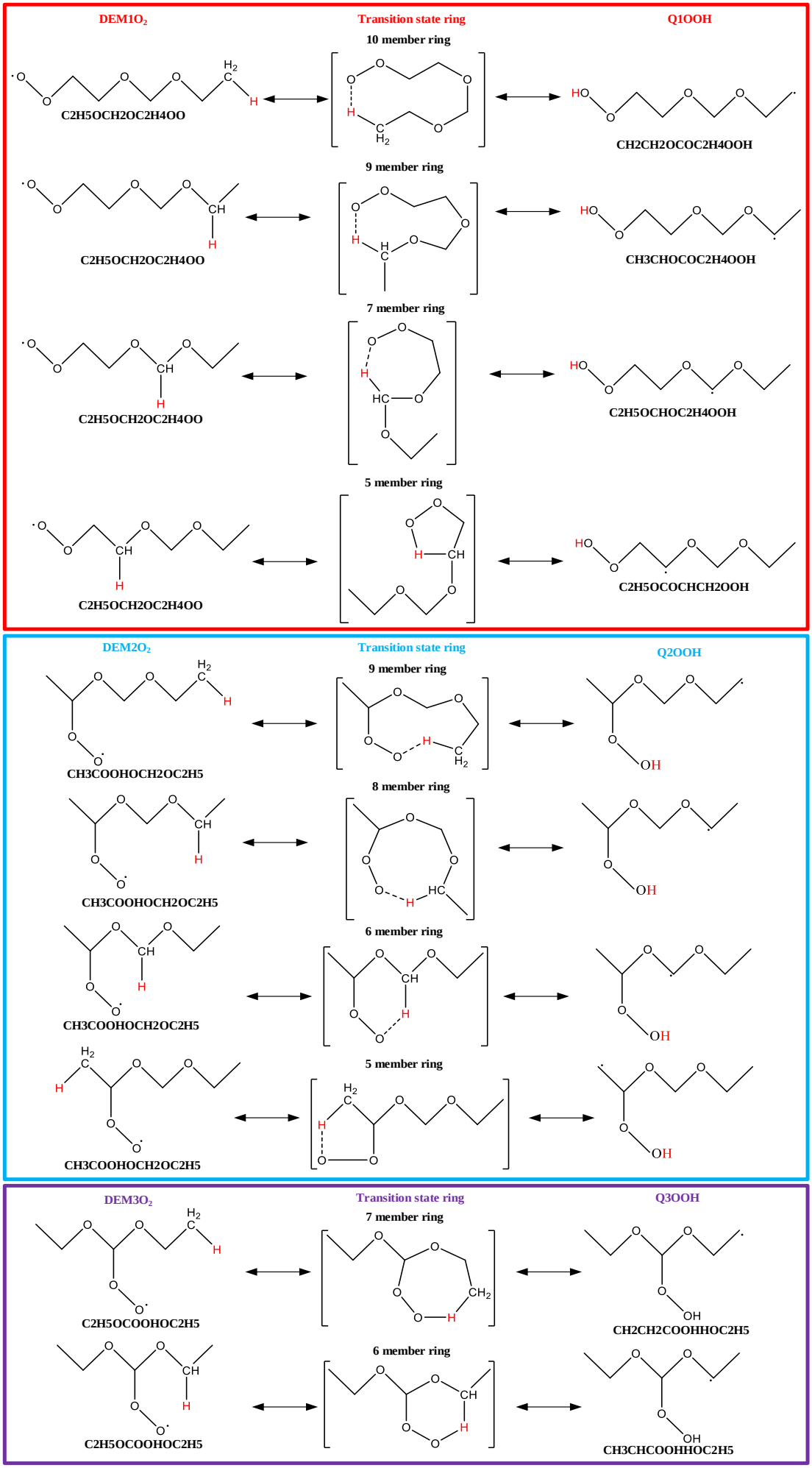

Fig. 7. Internal H-atom abstraction of $R\dot{O}_2$ radicals via transition state ring structure, reaction class 24: $R\dot{O}_2$ <=>QOOH.

Table 4. High temperature reaction classes considered in the DEM mechanism.

Class ID	High temperature reaction classes	Rate constant source					
		Aramco 3.0 [44]	DMM [38]	n-Heptane [30]	DEM [15, 16]	DEM [17]	This work
1	Unimolecular fuel decomposition: Fuel<=> $\dot{R}$ + $\ddot{R}$	√	√	×	√	√	√
2	Fuel decomposition: RH<=> $\dot{R}$ + $\dot{H}$	×	√	√	×	×	√
3	H-atom abstraction from the fuel by O_2/ $\dot{H}$ / $\dot{O}$ / $\dot{O}H$ / $H\dot{O}_2$ / $\dot{C}H_3$ / $CH_3\dot{O}$ / $CH_3\dot{O}_2$ / $\dot{O}_2CHO$ / $\dot{C}_2H_3$ / $\dot{C}_2H_5$ (primary/secondary carbon sites): RH+ $\dot{X}$ <=> $\dot{R}$ +XH	√	√	√	√	√	√
4	$\dot{R}$ radical decomposition	√	×	×	√	√	√
5	$\dot{R}$ radical isomerization	√	√	×	×	√	√
6	C–O: β-scission of $\dot{R}$ radicals	×	√	×	×	×	√
7	O–C–O: β-scission of $\dot{R}$ radicals	×	√	×	×	×	√
8	H-atom abstraction reactions from alkenes	√	×	×	×	×	√
9	Addition of radical species O and OH to alkenes	√	×	×	×	×	√
10	Reactions of alkenyl radicals with $H\dot{O}_2$, CH3O2, and C2H5O2	√	×	×	×	×	√
11	Alkenyl radical decomposition	√	×	×	×	×	√
12	Alkene decomposition	√	×	×	×	×	√
13	Retroene decomposition reactions	√	×	×	×	×	√

Table 5. Low temperature reaction classes considered in the DEM mechanism.

Class ID	Low-temperature reaction classes	Rate constant source					
		Aramco 3.0 [44]	DMM [38]	n-Heptane [30]	DEM [15, 16]	DEM [17]	This work
14	Addition of O_2 to $\dot{R}$ radicals: $\dot{R} + O_2 <=> R\dot{O}_2$	√	√	√	×	×	√
15	$\dot{R} + O_2 <=> E + H\dot{O}_2$ (E: radicals contain carbon-carbon double bond)	×	×	√	×	×	√
16	$\dot{R} + R'\dot{O}_2 <=> R\dot{O} + R'\dot{O}$ (including $\dot{R} + H\dot{O}_2 <=> R\dot{O} + OH$)	√	√	√	×	×	√
17	$R\dot{O}_2 + Fuel <=> ROOH + R'$	×	×	√	×	×	√
18	$R\dot{O}_2 + R'\dot{O}_2 <=> R\dot{O} + R'\dot{O} + O_2$ (including $R\dot{O}_2 + CH_3\dot{O}_2 <=> R\dot{O} + CH_3\dot{O} + O_2$)	√	×	√	×	×	√
19	$R\dot{O}_2 + H\dot{O}_2 <=> ROOH + O_2$	√	×	√	×	×	√
20	$R\dot{O}_2 + H_2O_2 <=> ROOH + H\dot{O}_2$	√	×	√	×	×	√
21	$ROOH <=> R\dot{O} + \dot{O}H$	×	×	√	×	×	√
22	$R\dot{O}$ decomposition	√	√	√	×	×	√
23	$R\dot{O}_2 <=> E + H\dot{O}_2$	×	×	√	×	×	√
24	$R\dot{O}_2$ radical isomerization: $R\dot{O}_2 <=> QOOH$	√	√	√	×	×	√
25	$R\dot{O}_2$ concerted eliminations: $R\dot{O}_2 <=> alkene + H\dot{O}_2$	√	×	×	√	×	√
26	QOOH = cyclic ether + OH (cyclic ether formation)	√	√	√	×	×	√
27	QOOH decomposition (β-scission products)	√	√	√	×	×	√
28	QOOH = alkene + HO2 (radical site beta to OOH group)	√	×	√	×	×	√
29	QOOH = ether with carbon-carbon double bond + HO2	×	×	×	×	×	√
30	QOOH = alkene + carbonyl + OH (radical site gamma to OOH group)	√	×	√	×	×	√
31	Addition of O_2 to $\dot{Q}OOH$: $\dot{Q}OOH + O_2 <=> \dot{O}_2QOOH$	√	√	√	×	×	√
32	$\dot{O}_2QOOH$ isomerization to form carbonylhydroperoxide and $\dot{O}H$	√	√	√	×	×	√
33	Carbonylhydroperoxide decomposition to form oxygenated radicals and $\dot{O}H$	√	√	√	×	×	√
34	Cyclic ether reactions with $\dot{O}H$ and $H\dot{O}_2$	√	√	√	×	×	√
35	Decomposition of large carbonyl species and carbonyl radicals	√	×	√	×	×	√
36	$\dot{O}_2QOOH <=> EROOH + H\dot{O}_2$ (EROOH: olefinic hydroperoxy)	×	×	√	×	×	√
37	EROOH decomposition	×	×	√	×	×	√

Table 6. Elementary reactions of H-atom abstract from fuel and rate constant for DEM and n-heptane [30].

DEM reactions	A ($cm^3mol^{-1}s^{-1}K^{-n}$)	n	E_a (cal/mole)	n-Heptane reactions	A ($cm^3mol^{-1}s^{-1}K^{-n}$)	n	E_a (cal/mole)
DEM+O2=DEM1+HO2	4.20E+13	1.7	52800	NC7H16+O2=C7H15-1+HO2	4.20E+13	0	52800
DEM+O2=DEM2+HO2	2.80E+13	1.7	50160	NC7H16+O2=C7H15-2+HO2	2.80E+13	0	50160
DEM+O2=DEM3+HO2	1.40E+13	1.7	50160	NC7H16+O2=C7H15-4+HO2	1.40E+13	0	50160
DEM+OH=DEM1+H2O	5.46E+07	3.513	868.4	NC7H16+OH=C7H15-1+H2O	2.73E+07	1.813	868.4
DEM+OH=DEM2+H2O	2.82E+10	2.635	504.7	NC7H16+OH=C7H15-2+H2O	1.41E+10	0.935	504.7
DEM+OH=DEM3+H2O	1.12E+12	2.02	846.5	NC7H16+OH=C7H15-4+H2O	5.62E+11	0.32	846.5
DEM+C2H5=DEM1+C2H6	1.00E+11	2	13400	NC7H16+C2H5=C7H15-1+C2H6	1.00E+11	0	13400
DEM+C2H5=DEM2+C2H6	1.00E+11	2	10400	NC7H16+C2H5=C7H15-2+C2H6	1.00E+11	0	10400
DEM+C2H5=DEM3+C2H6	5.00E+10	2	10400	NC7H16+C2H5=C7H15-4+C2H6	5.00E+10	0	10400

2.3 Thermochemical and transport data

The thermodynamic and transport parameters of the species are used to determine reverse rate constants. They are mainly taken from Aramco 3.0 mechanism [44], dimethoxymethane mechanism [38], n-heptane mechanism [30], DEM high temperature mechanism [15-17], 2-methylalkanes (C_7 to C_{20}) mechanism [31], dibutyl ether mechanism [36] and $PODE_{2-4}$ mechanism [40]. The thermochemical properties of species not present in the above mechanisms are calculated using group additivity theory proposed by Benson [50], Bozzelli et al. [51] and Glaude et al. [52]. The transport properties of unreported stable species are computed by the correlation proposed by Tee et al. [53]. The critical pressure, critical temperature, and acentric factor are needed to determine the Lennard-Jones potential well depth and collision diameter which are derived from Yaws' handbook [54], AP1700 Material property calculation and inquiry platform [55] and NIST Chemistry WebBook [46]. The transport properties of unreported radical species are adopted from radicals with identical chemical formulas and similar molecular structures or parent species.

3. RESULTS AND DISCUSSION

3.1 Ignition delay time validation

The full temperature regime (500~1400K) ignition delay times of DEM-air mixture at φ=1.0, P_{init}=30bar have been measured in shock tube (ST) and rapid compression machine (RCM) by Lehrheuer et al. [19]. The initial mixture compositions and boundary conditions are listed in Table 7. The comparison of the experimental data measured by Lehrheuer et al. [19] and prediction using the current UOB mechanism are plotted in Fig. 8. This kinetic model can reproduce the oxidation reactivity with varying initial gas temperature (500~1400K) and dilution ratio (N_2/O_2=3.76, 12). The NTC (negative temperature coefficient) behavior does not appear in the DEM ignition delay time profiles, but it emerges a shallow plateau at 620~920K when N_2/O_2=3.76. Similarly, the ignition delay time plateau presents at 580~840K when N_2/O_2 increases to 12. The DEM ignition delay times increases as dilution ratio N_2/O_2 increases from 3.76 to 12 while the intermediate temperature plateau moves toward lower temperature regime and narrows.

A sensitivity analysis on OH species respective to reaction A-factors is conducted at 500K, 800K, 1200K to identify the dominant reactions at low, intermediate, high temperature oxidation as shown in Fig. 9 (a) ~ Fig. 9 (c). The OH radical is the ignition indicator, accordingly those reactions with positive sensitivity coefficients promote OH radical production and enhance oxidation reactivity, vice versa. At T_{init}=500K, reaction sequence Eq. (8) ~ Eq. (10) is a main low temperature chain branching pathway. C_2H_5 is the β-scission product of DEM decomposition while CH_2O is the major β-scission product of oxygenated radicals (here refer to those formed by reaction class 33). H-atom abstraction by O_2, OH, HO_2, CH_3, CH_3O_2 and C_2H_5 from DEM to produce DEM2 (CH3CHOCH2OCH2CH3) all contribute to reactivity enhancement because after the 1st O_2 addition DEM2O2 (CH3COOHOCH2OC2H5) exists

four isomerized pathway. On the contrary, H-atom abstraction by OH, HO_2, CH_3, CH_3O_2 from DEM to form DEM3 (CH3CH2OCHOCH2CH3) inhibits oxidation reactivity because of t after the 1st O_2 addition. DEM3O2 (C2H5OCOOHOC2H5) has only two isomerization pathways. At T_{init}=800K, reaction sequence Eq. (11) ~ Eq. (15) is the main OH radical source to sustain the system reactivity. H-atom abstractions from DEM by CH_3 and C_2H_5 to form DEM2 and DEM3 are detrimental to OH radical accumulation as shown in Fig. 9 (b). DEMx takes place the 1st O_2 addition to produce DEMxO2 and sequentially isomerizes to form QOOH as shown in Fig. 4. But as the initial gas temperature exceeds 620K, QOOH reaction pathway would transfer from the 2nd O_2 addition toward QOOH decomposition to produce cyclic ether, ether with carbon double bond and β-scission products. At intermediate temperature, the low temperature chain branching reactions (reaction class 31, 32, 33) suspend and transfer to chain propagation reactions (reaction class 26, 27, 29). At 1200K, DEM decomposes by C-O bond fission (reaction class 1), it replaces H-atom abstraction from fuel (reaction class 3) becoming the major initiated reaction. The dominant OH radical formation pathway at a high temperature regime (above 920K) following the reaction sequence of Eq. (16) ~ Eq. (18), Eq. (15). While Eq. (19) consumes C2H5 radical which competes with the major OH radical production pathway, thus inhibits OH radical accumulation.

C2H5+O2<=>C2H5O2 (8)

C2H5O2+CH2O<=>C2H5O2H+HCO (9)

C2H5O2H<=>C2H5O+OH (10)

C2H5+O2<=>C2H5O2 (11)

C2H5O2<=>CH3CHO+OH (12)

CH3CHO+HO2<=>CH3CO+H2O2 (13)

CH3CHO+CH3O2<=>CH3CO+CH3O2H (14)

H2O2(+M)<=>2OH(+M) (15)

DEM<=>C2H5OCH2O+C2H5 (16)

C2H5OCH2O<=>C2H5O+CH2O (17)

CH2O+HO2<=>HCO+H2O2 (18)

DEM+C2H5<=>CH3CH2OCHOCH2CH3+C2H6 (19)

The high temperature regime (1100~1400K) ignition delay times of DEM/O_2/Ar mixture at φ=0.5/1.0/2.0, P_{init}=2/4/10bar have been measured in shock tube (ST) by Zhang et al. [17]. UCL mechanism proposed by Dias et al. [15, 16] is developed and validated against 50mbar and does not apply to the pressure range of 2~10bar. So the simulation results of the current UOB mechanism and SCU mechanism proposed by Zhang et al. [17] are validated against shock tube ignition delay times as shown in Fig. 10. Both mechanisms have their advantages and disadvantages: (1) current UOB mechanism is more specific to engine relevant pressure and the discrepancy reduces as increasing initial pressure; (2) current UOB mechanism obtains high predictive accuracy at stoichiometric and fuel-rich conditions and under-estimates the oxidation reactivity at fuel-lean condition; (3) the experimental ignition delay times below 1160K are better reproduced by current UOB mechanism than SCU mechanism [17]. This work incorporates both low temperature and high temperature reaction classes while the SCU mechanism [17] contains only high temperature reaction classes. UCL mechanism proposed by Dias et al. [15, 16] confronts the same issue as the SCU mechanism [17], hence both mechanisms do not apply to ignition delay time validation over the full temperature regime in Fig. 8.

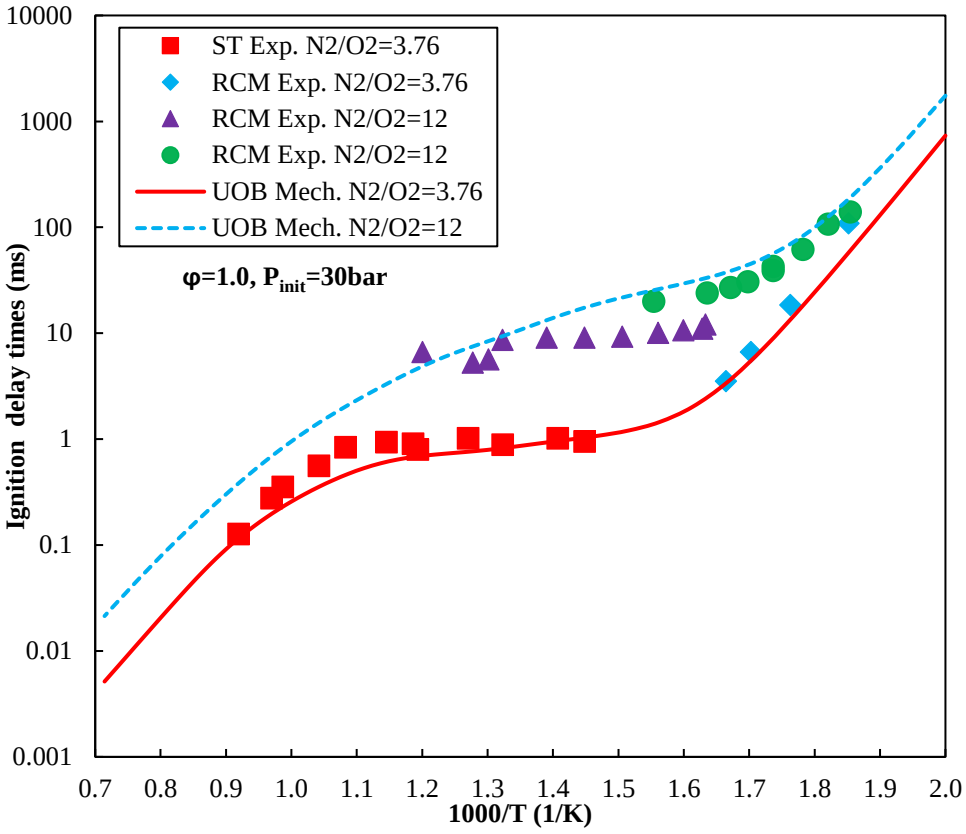

328

329 **Fig. 8.** Experimental (symbols [19]) and modeling results (lines) for DEM ignition delay times at φ=1.0,

330 T_{init}=500~1400K, P_{init}=30bar.

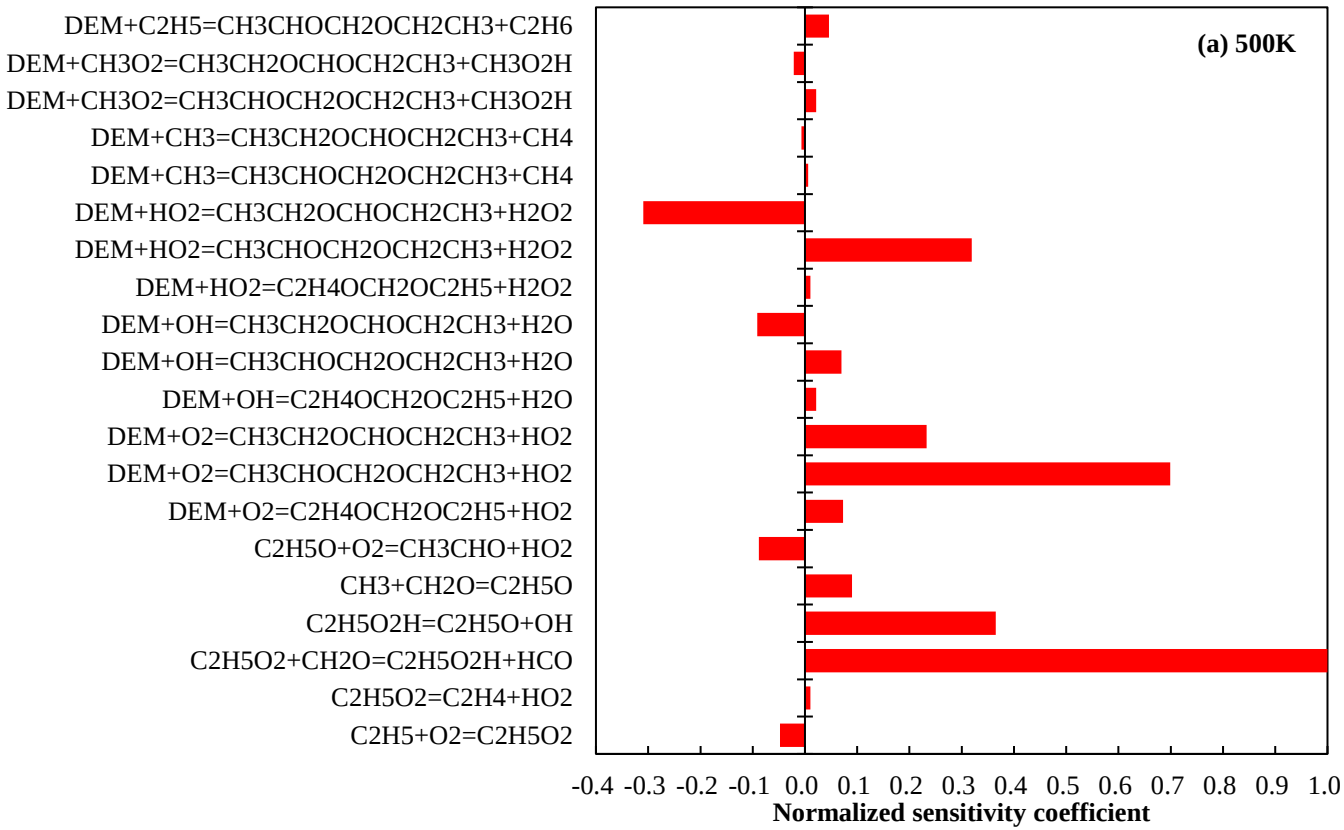
DEM+C2H5=CH3CHOCH2OCH2CH3+C2H6
DEM+CH3O2=CH3CH2OCHOCH2CH3+CH3O2H
DEM+CH3O2=CH3CHOCH2OCH2CH3+CH3O2H
DEM+CH3=CH3CH2OCHOCH2CH3+CH4
DEM+CH3=CH3CHOCH2OCH2CH3+CH4
DEM+HO2=CH3CH2OCHOCH2CH3+H2O2
DEM+HO2=CH3CHOCH2OCH2CH3+H2O2
DEM+HO2=C2H4OCH2OC2H5+H2O2
DEM+OH=CH3CH2OCHOCH2CH3+H2O
DEM+OH=CH3CHOCH2OCH2CH3+H2O
DEM+OH=C2H4OCH2OC2H5+H2O
DEM+O2=CH3CH2OCHOCH2CH3+HO2
DEM+O2=CH3CHOCH2OCH2CH3+HO2
DEM+O2=C2H4OCH2OC2H5+HO2
C2H5O+O2=CH3CHO+HO2
CH3+CH2O=C2H5O
C2H5O2H=C2H5O+OH
C2H5O2+CH2O=C2H5O2H+HCO
C2H5O2=C2H4+HO2
C2H5+O2=C2H5O2
(a) 500K
-0.4 -0.3 -0.2 -0.1 0.0 0.1 0.2 0.3 0.4 0.5 0.6 0.7 0.8 0.9 1.0
Normalized sensitivity coefficient

331

332

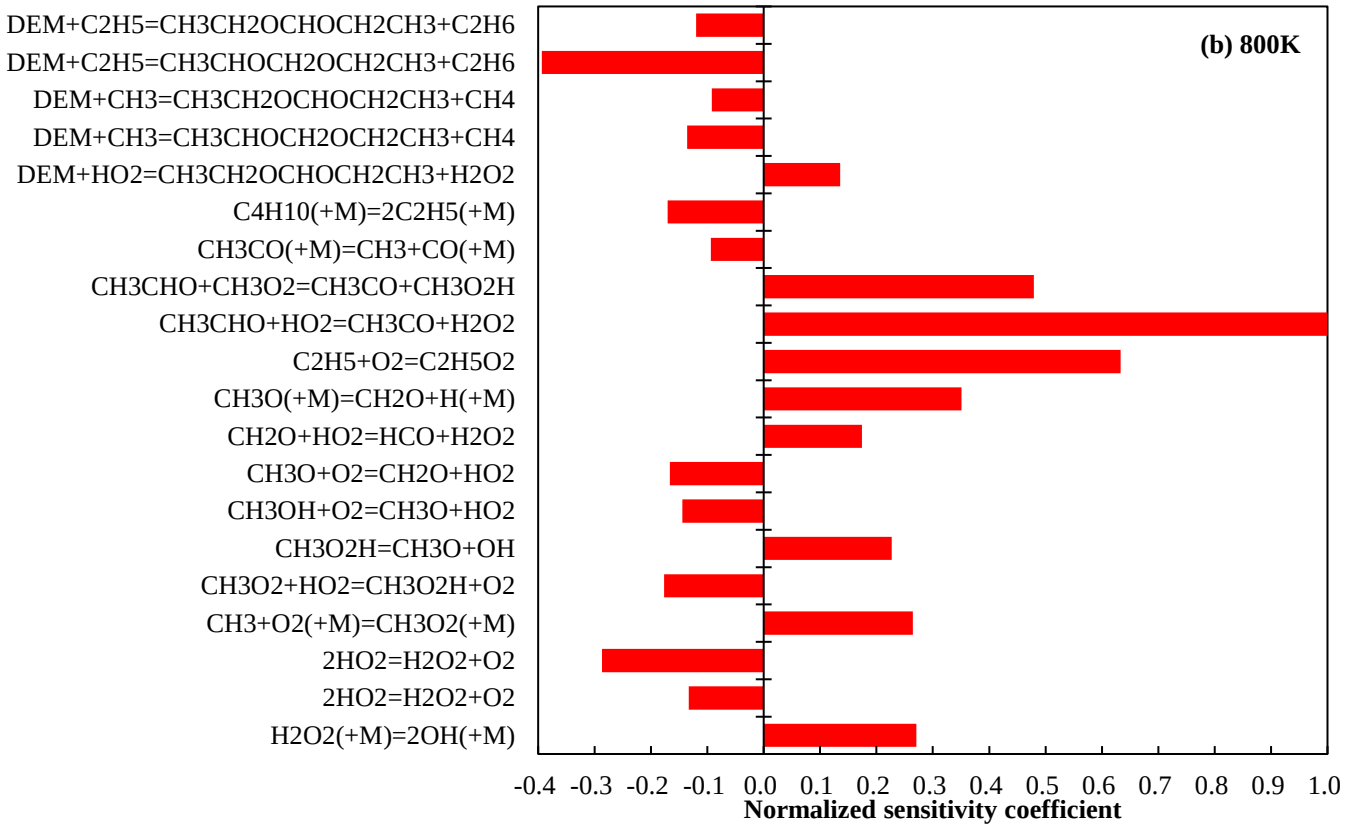
DEM+C2H5=CH3CH2OCHOCH2CH3+C2H6
DEM+C2H5=CH3CHOCH2OCH2CH3+C2H6
DEM+CH3=CH3CH2OCHOCH2CH3+CH4
DEM+CH3=CH3CHOCH2OCH2CH3+CH4
DEM+HO2=CH3CH2OCHOCH2CH3+H2O2
C4H10(+M)=2C2H5(+M)
CH3CO(+M)=CH3+CO(+M)
CH3CHO+CH3O2=CH3CO+CH3O2H
CH3CHO+HO2=CH3CO+H2O2
C2H5+O2=C2H5O2
CH3O(+M)=CH2O+H(+M)
CH2O+HO2=HCO+H2O2
CH3O+O2=CH2O+HO2
CH3OH+O2=CH3O+HO2
CH3O2H=CH3O+OH
CH3O2+HO2=CH3O2H+O2
CH3+O2(+M)=CH3O2(+M)
2HO2=H2O2+O2
2HO2=H2O2+O2
H2O2(+M)=2OH(+M)
(b) 800K
-0.4 -0.3 -0.2 -0.1 0.0 0.1 0.2 0.3 0.4 0.5 0.6 0.7 0.8 0.9 1.0
Normalized sensitivity coefficient

333

334

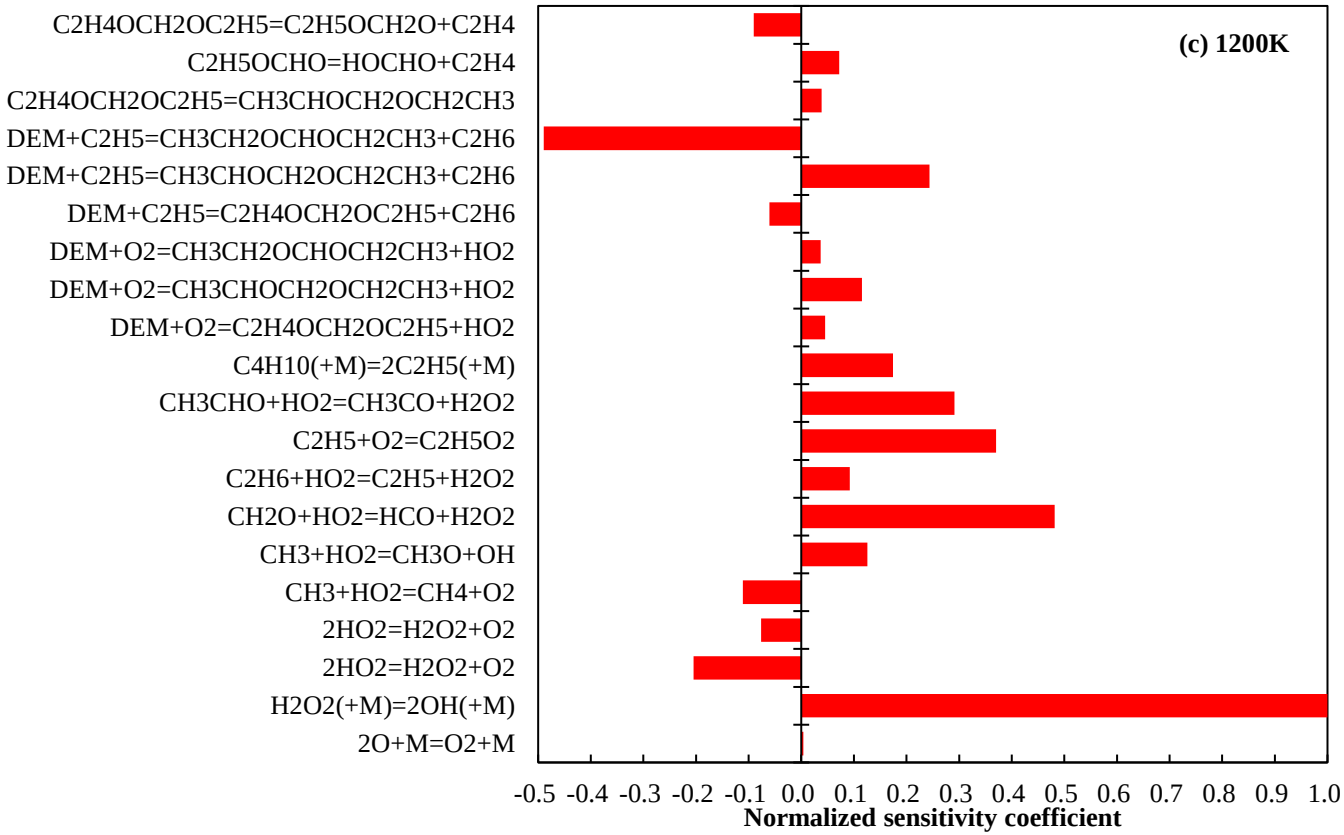

335

336 **Fig. 9.** Sensitivity analysis on OH species respective to reaction A-factors for DEM oxidation at φ=1.0, T_{init}=500/800/1200K, P_{init}=30bar, N_2/O_2=3.76.

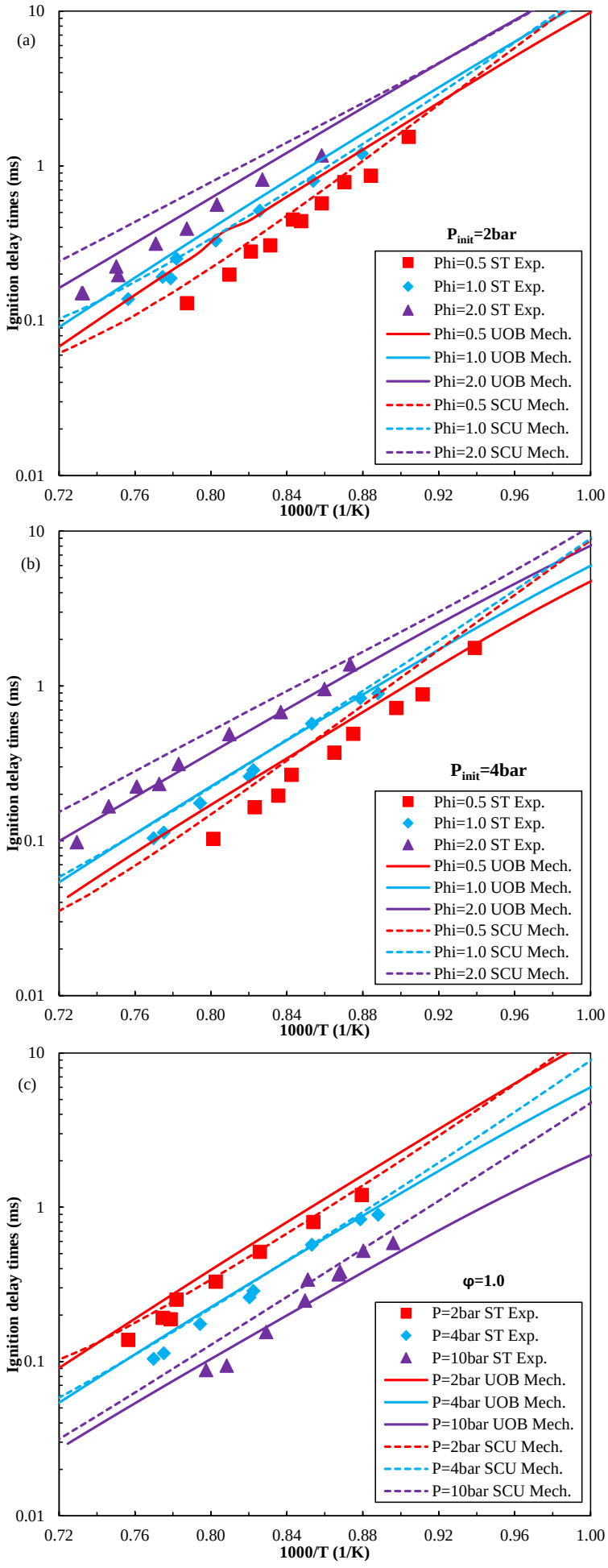

Fig. 10. Experimental (symbols [17]) and modeling results (lines) of DEM/O_2/Ar mixture ignition delay times at φ=0.5/1.0/2.0, T_{init}=1000~1400K, P_{init}=2/4/10bar.

340 **Table 7. Boundary conditions of DEM oxidation for ignition delay time experiments/simulations**

	Compositions	φ	T_{init} (K)	P_{init} (bar)
Lehrheuer er al. [19]	DEM:O2:N2=1:7:26.32	1.0	500~1400	30
	DEM:O2:N2=1:7:84	1.0	500~1400	30
Zhang et al. [17]	DEM:O2:Ar=1:14:85	0.5	1000~1400	2/4
	DEM:O2:Ar=1:7:92	1.0	1000~1400	2/4/10
	DEM:O2:Ar=1:3.5:95.5	2.0	1000~1400	2/4

341

3.2 Laminar flame speed validation

The current UOB mechanism has been validated against the premixed laminar flame speed of DEM-air mixture at φ=0.5~2.0, T_{init}= 1atm, P_{init}=1.01/2.50bar reported by Kopp. et al. [20]. The comparisons are plotted in Fig. 11. The high temperature version UOB mechanism is adopted to simulate the flame phenomenon which removes the low-temperature species and reactions to accelerate the computational speed. The dependence of flame speed on equivalence ratio is well captured by the current UOB mechanism except for the impact of initial gas pressure. Current UOB mechanism overestimates the flame speed by 2.8cm/s at φ=1.1, P_{init}=1.01bar while under-estimates the flame speed by 1.5cm/s at φ=1.1, P_{init}=2.50bar. This deviation becomes more distinct at φ=1.5, P_{init}=2.50bar and it causes difficulty in reaction rate constant calibration. More experimental flame speed data are required to refine the kinetic model and reduce experimental uncertainty.

The peak flame speed appears at φ=1.1 under 1.01bar and 2.50bar as shown in Fig. 11. Sensitivity analysis on laminar flame speed respective to reaction A-factors is conducted to distinguish the dominant reactions at φ=0.8/1.1/1.5 as shown in Fig. 12 (a) ~ Fig. 12 (c). High temperature chain branching reaction H+O2<=>O+OH are the dominant reaction of flame speed at varying equivalence ratio. And CO+OH<=>CO2+H is the secondary dominant reaction to enhance the flame speed at φ=0.8 and φ=1.1 which are also the major heat release reaction. Especially, H-atom abstraction from DEM by C_2H_5 to produce DEM3 benefit the flame speed acceleration at the fuel-lean condition. This further supports that C_2H_5 radicals play a key role in DEM decomposition by reaction class 1 and reaction class 3. At fuel-rich conditions (φ=1.5), HCO+M<=>CO+H+M replace CO+OH<=>CO2+H becoming the major heat release reaction to promote flame speed due to oxygen deficiency. Endothermic reaction H2O+M<=>H+OH+M and chain termination reaction CH3+H(+M)<=>CH4(+M) decrease reaction

364 temperature and retard the active radical accumulation, thus contributes to flame speed reduction.

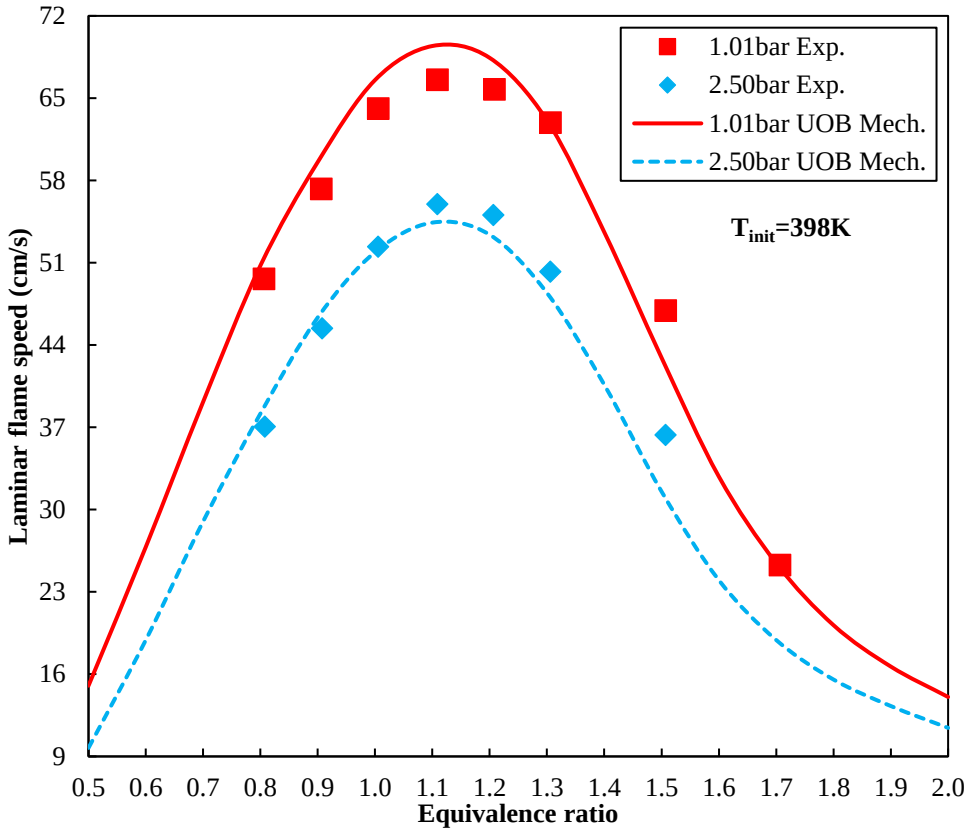

365

366 **Fig. 11.** Experimental (symbols [20]) and modeling results (lines) for the laminar flame speed of DEM

367 in air at φ=0.5~2.0, T_{init}= 1atm, P_{init}=1.01/2.50bar.

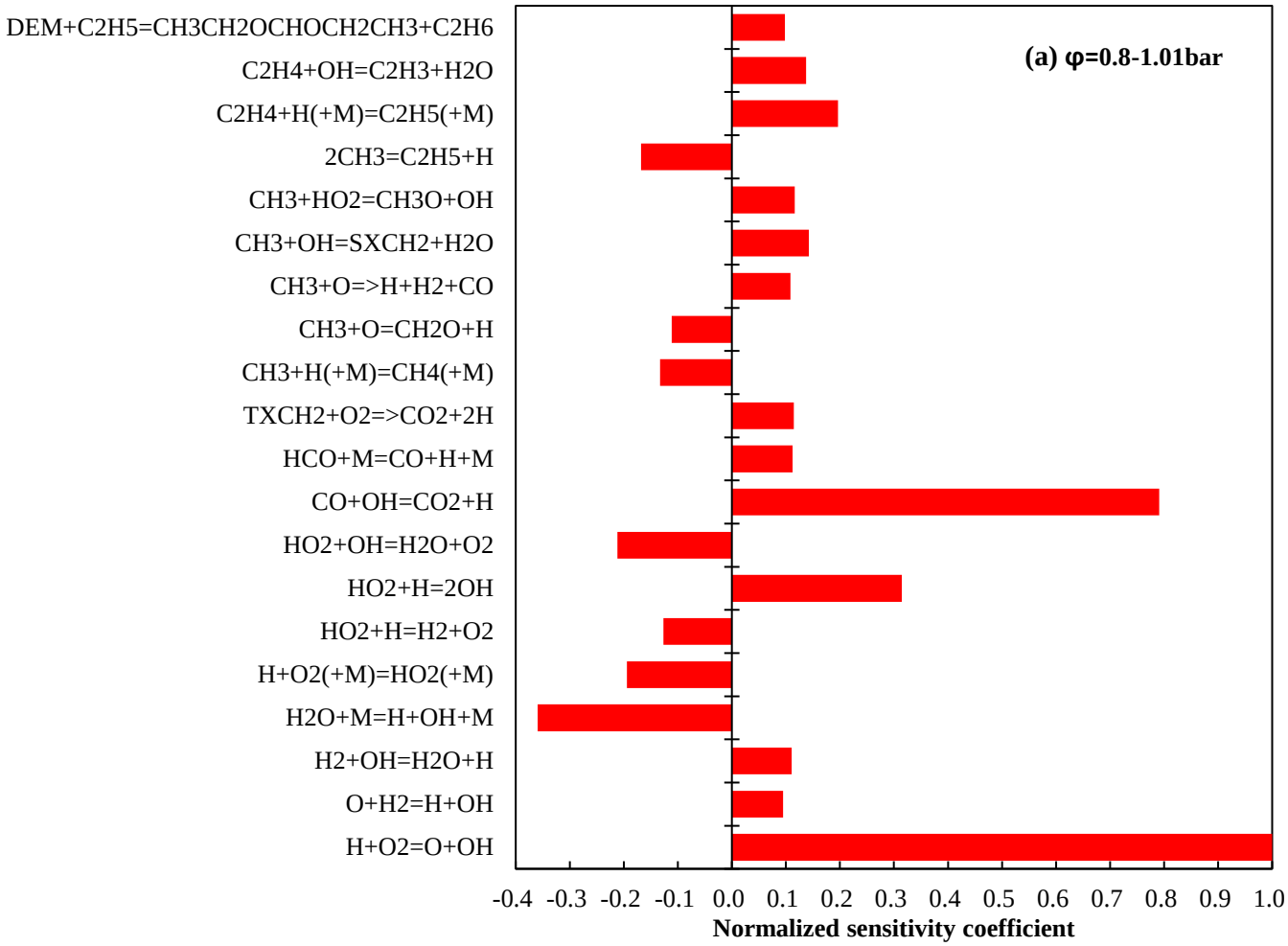
DEM+C2H5=CH3CH2OCHOCH2CH3+C2H6
C2H4+OH=C2H3+H2O
C2H4+H(+M)=C2H5(+M)
2CH3=C2H5+H
CH3+HO2=CH3O+OH
CH3+OH=SXCH2+H2O
CH3+O=>H+H2+CO
CH3+O=CH2O+H
CH3+H(+M)=CH4(+M)
TXCH2+O2=>CO2+2H
HCO+M=CO+H+M
CO+OH=CO2+H
HO2+OH=H2O+O2
HO2+H=2OH
HO2+H=H2+O2
H+O2(+M)=HO2(+M)
H2O+M=H+OH+M
H2+OH=H2O+H
O+H2=H+OH
H+O2=O+OH
(a) φ=0.8-1.01bar
-0.4 -0.3 -0.2 -0.1 0.0 0.1 0.2 0.3 0.4 0.5 0.6 0.7 0.8 0.9 1.0
Normalized sensitivity coefficient

368

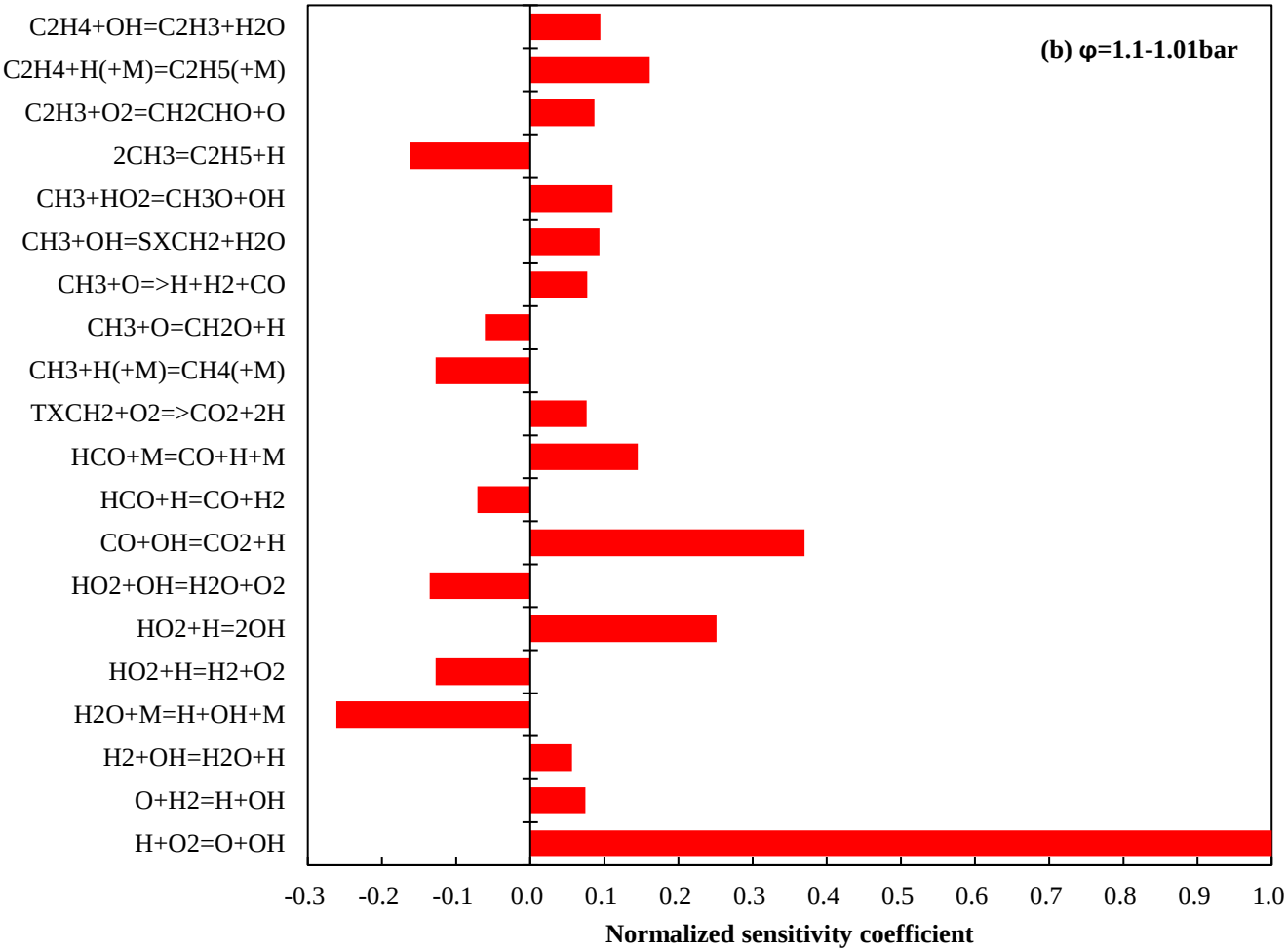
(b) φ=1.1-1.01bar
C2H4+OH=C2H3+H2O
C2H4+H(+M)=C2H5(+M)
C2H3+O2=CH2CHO+O
2CH3=C2H5+H
CH3+HO2=CH3O+OH
CH3+OH=SXCH2+H2O
CH3+O=>H+H2+CO
CH3+O=CH2O+H
CH3+H(+M)=CH4(+M)
TXCH2+O2=>CO2+2H
HCO+M=CO+H+M
HCO+H=CO+H2
CO+OH=CO2+H
HO2+OH=H2O+O2
HO2+H=2OH
HO2+H=H2+O2
H2O+M=H+OH+M
H2+OH=H2O+H
O+H2=H+OH
H+O2=O+OH
-0.3
-0.2
-0.1
0.0
0.1
0.2
0.3
0.4
0.5
0.6
0.7
0.8
0.9
1.0
Normalized sensitivity coefficient

369

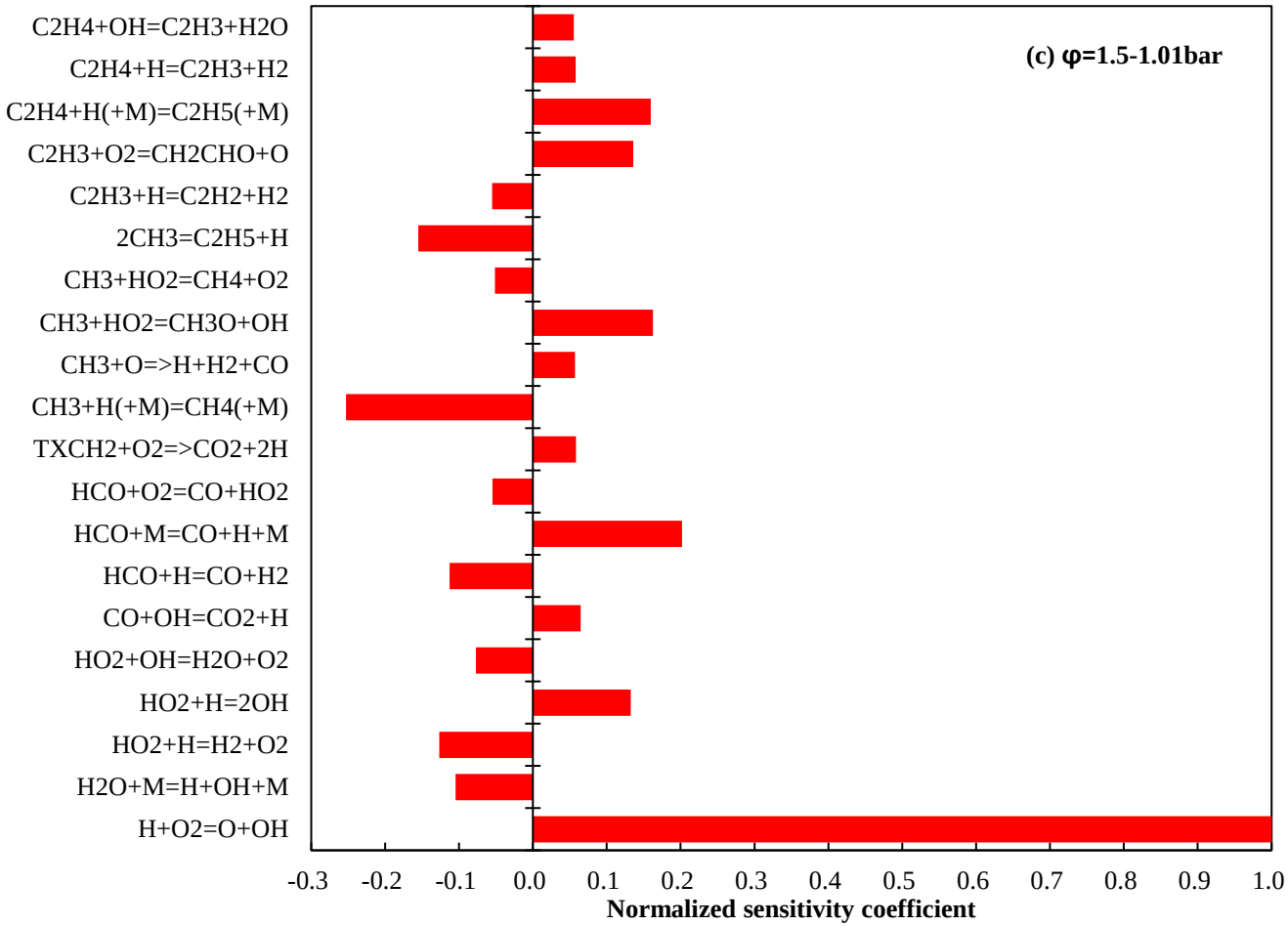

Fig. 12. Sensitivity analysis on laminar flame speed respective to reaction A-factors for DEM oxidation at T_{init}=398K, P_{init}=1.01bar, (a) φ=0.8, (b) φ=1.1, (c) φ=1.5.

3.3 Comparison of ignition delay times between DEM and n-heptane

The oxidation reactivity between DEM and n-heptane is examined at φ=0.25 ~ 2.0, T_{init}= 500~1400K, P_{init}= 13.5 ~ 55bar as shown in Fig. 13 and the boundary conditions are chosen from ref. [56, 57]. The DEM ignition delay times have three characteristics: (1) It decreases with increasing initial pressure and equivalence ratio under 500~1400K being similar to n-heptane. (2) The ignition delay time profiles exist a wide shallow plateau at a temperature range of 620~960K and the plateau narrows as the equivalence ratio decreases from 2.0 to 0.5. A weak NTC region appears until the equivalence ratio further decreases to 0.25 and it moves towards higher temperature as increasing pressure. On the contrary, n-heptane demonstrates NTC behavior for all studied conditions. (3) DEM has greater low temperature oxidation reactivity than n-heptane thus its ignition delay times are lower than n-heptane at 500~670K. The species evolution of the DEM and n-heptane ignition process at low (560K)/intermediate (800K)/high temperature (1200K) are illustrated in Fig. 14. The DEM ignition process has two key characteristics:

(i) The low temperature heat release (LTHR) intensity of DEM is weaker than n-heptane being similar to $PODE_3$ reported by Li et al. [41]. The initiated temperature and amplitude of DEM LTHR are 575K and 205K while those of n-heptane are 832K and 316K respectively. From the perspective of active radical pool production, DEM completes 45.13% H_2O_2 accumulation at LTHR while n-heptane reaches 87.86%. DEM has greater low temperature oxidation reactivity (namely low ignition delay times) but the LTHR intensity (temperature increase) and active radical accumulation are not sufficient. Therefore, DEM is not appropriate to undertake the role of chemical ignition source compared to n-heptane which is similar to $PODE_3$ (polyoxymethylene dimethyl ether 3).

(ii) The DEM heat release process transits from two-stage heat release (LTHR+HTHR) to single-

394 stage heat release (HTHR) as the initial gas temperature increases from 500 to 1400K. There
395 is no distinct LTHR stage at intermediate temperature (640~940) which is different from n-
396 heptane as shown in Fig. 14 (b) and Fig. 14 (e).

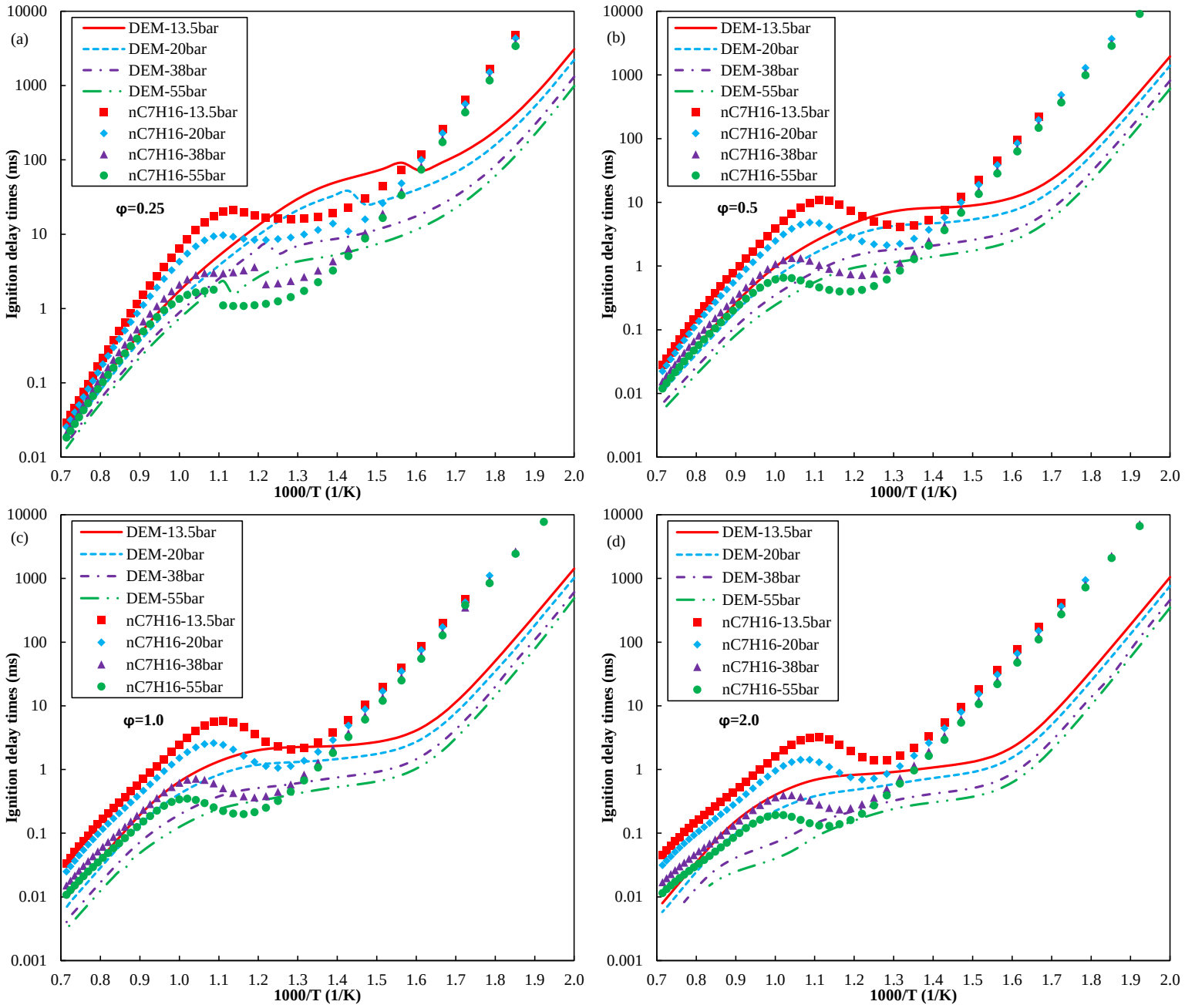

Fig. 13. Ignition delay times of DEM-air mixture and n-heptane-air mixture at T_{init}= 500~1400K, P_{init}= 13.5, 20, 38, 55bar, (a) φ=0.25, (b) φ=0.5, (c) φ=1.0, (d) φ=2.0.

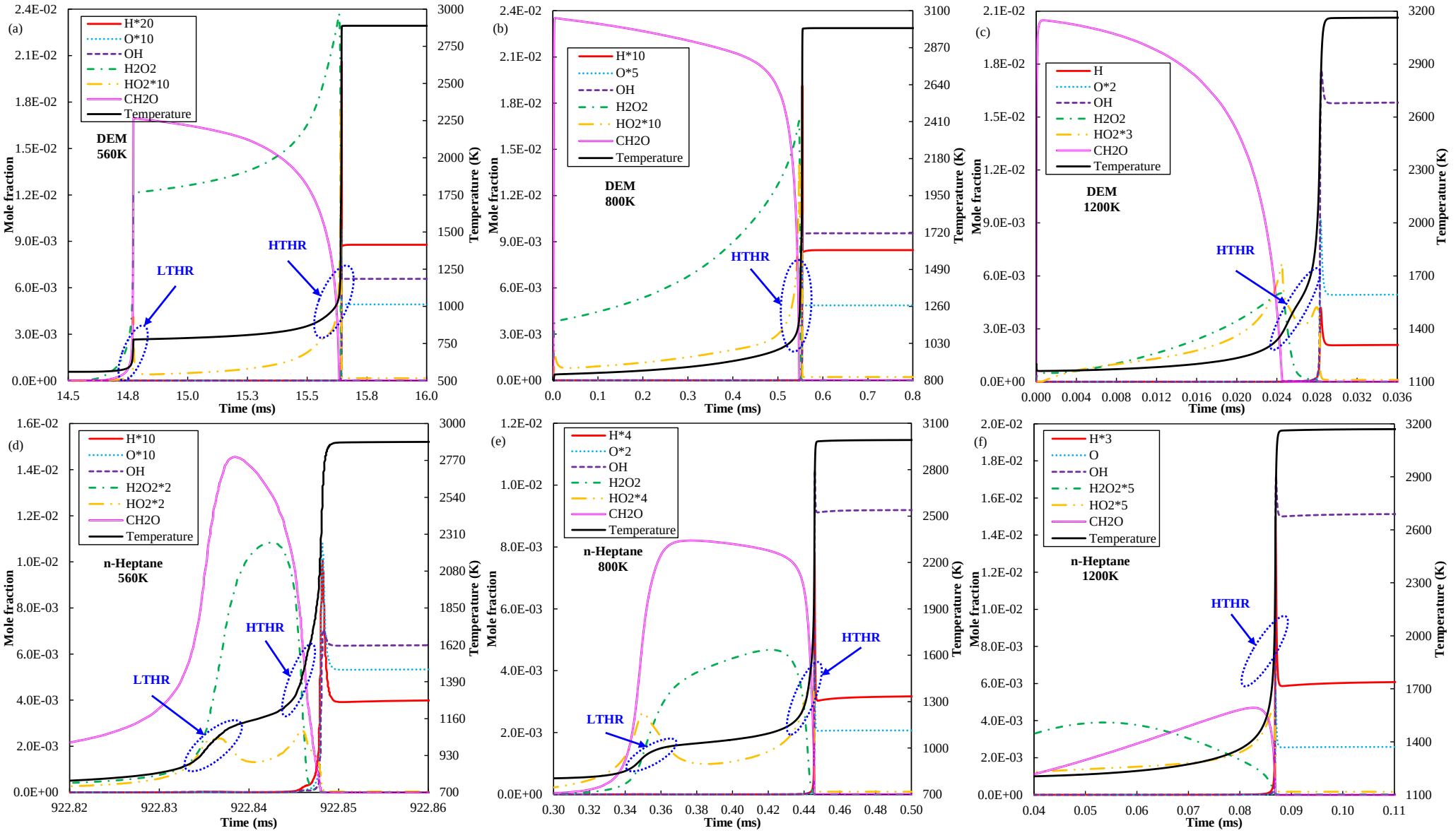

Fig. 14. Species evolution of DEM-air mixture and n-heptane-air mixture at φ=1.0, P_{init}= 38bar, (a)/(d) T_{init}= 560K, (b)/(e) T_{init}= 800K, (c)/(f) T_{init}= 1200K.

4. CONCLUSIONS

A detailed reaction mechanism for diethoxymethane (DEM) oxidation covering low and high temperature reactions is first reported in this study. The DEM low temperature reaction scheme is designed by analogy method based on the updated n-heptane mechanism while the high temperature reaction scheme follows the published DEM mechanisms. The reaction rate rules are consistent with Aramco 3.0 mechanism which is taken as a base mechanism to consider the C0-C4 fuels, C1-C3 alcohols, n-pentane and their isomers, n-hexane, mano-aromatics and PAHs. Dimethoxymethane mechanism is also introduced to ensure the compatibility between DEM sub-mechanism and Aramco 3.0 base mechanism and adopted the same reaction rate rule. The thermodynamic and transport parameters for new species in DEM sub-mechanism are determined by the group additivity method and properties correlation method. This mechanism has been successfully validated against the macroscopic combustion parameters of ignition delay times and laminar flame speed which are measured by shock tube/rapid compression machine and spherical flame in constant volume vessel. A reasonable agreement between experimental observation and numerical results is obtained, thus the reaction scheme should be reasonably correct. But the rate constants of the DEM low temperature reactions computed by the quantum chemistry and transition state theory are highly recommended in future research to reduce the mechanism uncertainty. Besides, the experimental data of species profiles measured in the jet-stirred reactor is needed for mechanism development and validation in the future.

A thorough comparison on the ignition delay times between DEM and n-heptane is conducted and it reveals that: (i) DEM is more reactive at low temperature (500~670K) oxidation compared to n-heptane which makes DEM an ideal carbon-neutral fuel for low temperature combustion (LTC) mode. (ii) The DEM ignition delay times exhibit a monotonous temperature dependence at the full temperature regime

(500~1400K) which also favors LTC mode. NTC behavior only occurs at φ=0.25 and the negative slope is weak. (3) DEM may not be a good chemical ignition source compared to n-heptane due to the insufficient temperature increase and active radical accumulation at the low temperature heat release stage. A similar conclusion is also reported for $PODE_3$ (polyoxymethylene dimethyl ether 3) which is an ether with multiple oxygen atoms.

ACKNOWLEDGEMENT

This work is supported by Innovate UK (The Technology Strategy Board, TSB, No. 400176/149) and Engineering & Physical Sciences Research Council (EPSRC, No. EP/P03117X/1). Runzhao Li also thanks to University of Birmingham for the award of a Ph.D. research scholarship (No. 1871018). This work is conducted in Future Engines & Fuels Lab, University of Birmingham. Special appreciations go to Dr. Véronique Dias in Institute of Mechanics, Materials and Civil Engineering (IMMC), Université catholique de Louvain for her invaluable discussion and guidance on diethoxymethane mechanism development in this work. The authors also thank Shenzhen Gas Corporation Ltd. for providing us the technical guidance. The authors are indebted to the reviewers of this article for their invaluable suggestions.

REFERENCES

[1] Bui M, Adjiman CS, Bardow A, Anthony EJ, Boston A, Brown S, et al. Carbon capture and storage (CCS): the way forward. Energy & Environmental Science 2018;11(5):1062-176.

[2] Nørskov JK, Latimer A, Dickens CF. Research needs towards sustainable production of fuels and chemicals. ENERGY-X 2019:https://www.energy-x.eu/research-needs-report/.

[3] SUNERGY.https://www.sunergy-initiative.eu/.

[4] Solar Fuels Network.https://www.solarfuelsnetwork.com/.

[5] Bossmann T, Fournié L, Humberset L, Khallouf P. The role and potential of Power-to-X in 2050. 2019.

[6] Kopernikus project P2X.https://www.kopernikus-projekte.de/en/projects/p2x.

[7] Soler A. Role of e-fuels in the European transport system-literature review. 2020:https://www.concawe.eu/publication/role-of-e-fuels-in-the-european-transport-system-literature-review/.

[8] Leitner W, Klankermayer J, Pischinger S, Pitsch H, Kohse-Hoinghaus K. Advanced Biofuels and Beyond: Chemistry Solutions for Propulsion and Production. Angew Chem Int Ed Engl 2017;56(20):5412-52.

[9] Beydoun K, Klankermayer J. Cover Feature: Ruthenium-Catalyzed Synthesis of Cyclic and Linear Acetals by the Combined Utilization of CO2, H2, and Biomass Derived Diols (Chem. Eur. J. 49/2019). Chemistry – A European Journal 2019;25(49):11392-.

[10] Farrell J, Wagner R, Gaspar D, Moen C. Co-Optimization of Fuels & Engines FY18 Year in Review. 2018:https://www.energy.gov/sites/prod/files/2019/06/f64/Co-

461 Optima_YIR8_FINAL_LOWRES%20190619_0.pdf.
462 [11] Wagner R, Gaspar D, Bryan P, McCormick R. Co-Optimization of Fuels & Engines FY19 Year
463 in Review. 2019:https://www.energy.gov/sites/prod/files/2020/06/f75/beto-co-optima-fy19-yir-
464 report-june-.pdf.
465 [12] Farrell J, Wagne R, Moen C, Gaspar D. A Transportation Future with Science in the Driver's Seat:
466 Mapping a Viable Route Forward for Affordable, Efficient, and Clean Fuels and Engines. National
467 Renewable Energy Laboratory 2020:https://www.energy.gov/sites/prod/files/2020/04/f73/beto-
468 co-optima-capstone-report-mar-.pdf.
469 [13] Yanowitz J, Ratcliff MA, McCormick RL, Taylor JD, Murphy MJ. Compendium of Experimental
470 Cetane Numbers. 2017.
471 [14] Thenert K, Beydoun K, Wiesenthal J, Leitner W, Klankermayer J. Ruthenium-Catalyzed
472 Synthesis of Dialkoxymethane Ethers Utilizing Carbon Dioxide and Molecular Hydrogen.
473 Angewandte Chemie 2016;128(40):12454-7.
474 [15] Dias V, Vandooren J. Experimental and modeling studies of C2H4/O2/Ar, C2H4/methylal/O2/Ar
475 and C2H4/ethylal/O2/Ar rich flames and the effect of oxygenated additives. Combustion and
476 Flame 2011;158(5):848-59.
477 [16] Dias V, Vandooren J, Jeanmart H. Experimental and Modeling Study of Propanal/H2/O2/Ar
478 Flames at Low Pressure. Combustion Science and Technology 2016;188(4-5):556-70.
479 [17] Zhang C, He J, Li Y, Li X, Li P. Ignition delay times and chemical kinetics of
480 diethoxymethane/O2/Ar mixtures. Fuel 2015;154:346-51.
481 [18] Kröger LC, Döntgen M, Firaha D, Kopp WA, Leonhard K. Ab initio kinetics predictions for H-
482 atom abstraction from diethoxymethane by hydrogen, methyl, and ethyl radicals and the

subsequent unimolecular reactions. Proceedings of the Combustion Institute 2019;37(1):275-82.

[19] Lehrheuer B, Hoppe F, Heufer KA, Jacobs S, Minwegen H, Klankermayer J, et al. Diethoxymethane as tailor-made fuel for gasoline controlled autoignition. Proceedings of the Combustion Institute 2019;37(4):4691-8.

[20] Kopp WA, Kröger LC, Cai L, Hesse R, Kruse S, Alquaity ABS, et al. Combustion Chemistry of Diethoxymethane (DEM): Experiments, Theory and Modeling. The 6th Fuel Science-From Production to Propulsion 2018.

[21] Battin-Leclerc F, Simmie JM, Blurock E. Cleaner Combustion: Developing Detailed Chemical Kinetic Models. London: Springer; 2013.

[22] Westbrook CK, Mehl M, Pitz WJ, Kukkadapu G, Wagnon S, Zhang K. Multi-fuel surrogate chemical kinetic mechanisms for real world applications. Phys Chem Chem Phys 2018;20(16):10588-606.

[23] Curran HJ, Gaffuri P, Pitz WJ, Westbrook CK. A Comprehensive Modeling Study of n-Heptane Oxidation. Combustion and Flame 1998;114(1-2):149-77.

[24] Lu T, Law CK. Toward accommodating realistic fuel chemistry in large-scale computations. Progress in Energy and Combustion Science 2009;35(2):192-215.

[25] Hashemi H, Christensen JM, Harding LB, Klippenstein SJ, Glarborg P. High-pressure oxidation of propane. Proceedings of the Combustion Institute 2019;37(1):461-8.

[26] Baigmohammadi M, Patel V, Nagaraja S, Ramalingam A, Martinez S, Panigrahy S, et al. Comprehensive Experimental and Simulation Study of the Ignition Delay Time Characteristics of Binary Blended Methane, Ethane, and Ethylene over a Wide Range of Temperature, Pressure, Equivalence Ratio, and Dilution. Energy & Fuels 2020;34(7):8808-23.

[27] Mohamed AAE-S, Panigrahy S, Sahu AB, Bourque G, Curran H. An experimental and kinetic modeling study of the auto-ignition of natural gas blends containing C1–C7 alkanes. Proceedings of the Combustion Institute 2020.

[28] Bugler J, Rodriguez A, Herbinet O, Battin-Leclerc F, Togbé C, Dayma G, et al. An experimental and modelling study of n-pentane oxidation in two jet-stirred reactors: The importance of pressure-dependent kinetics and new reaction pathways. Proceedings of the Combustion Institute 2017;36(1):441-8.

[29] Bugler J, Marks B, Mathieu O, Archuleta R, Camou A, Grégoire C, et al. An ignition delay time and chemical kinetic modeling study of the pentane isomers. Combustion and Flame 2016;163:138-56.

[30] Zhang K, Banyon C, Bugler J, Curran HJ, Rodriguez A, Herbinet O, et al. An updated experimental and kinetic modeling study of n-heptane oxidation. Combustion and Flame 2016;172:116-35.

[31] Sarathy SM, Westbrook CK, Mehl M, Pitz WJ, Togbe C, Dagaut P, et al. Comprehensive chemical kinetic modeling of the oxidation of 2-methylalkanes from C7 to C20. Combustion and Flame 2011;158(12):2338-57.

[32] Shrestha KP, Eckart S, Elbaz AM, Giri BR, Fritsche C, Seidel L, et al. A comprehensive kinetic model for dimethyl ether and dimethoxymethane oxidation and NO interaction utilizing experimental laminar flame speed measurements at elevated pressure and temperature. Combustion and Flame 2020;218:57-74.

[33] vom Lehn F, Cai L, Pitsch H. Impact of thermochemistry on optimized kinetic model predictions: Auto-ignition of diethyl ether. Combustion and Flame 2019;210:454-66.

527 [34] Sakai Y, Herzler J, Werler M, Schulz C, Fikri M. A quantum chemical and kinetics modeling study
528 on the autoignition mechanism of diethyl ether. Proceedings of the Combustion Institute
529 2017;36(1):195-202.
530 [35] Serinyel Z, Lailliau M, Dayma G, Dagaut P. A high pressure oxidation study of di-n-propyl ether.
531 Fuel 2020;263.
532 [36] Thion S, Togbé C, Serinyel Z, Dayma G, Dagaut P. A chemical kinetic study of the oxidation of
533 dibutyl-ether in a jet-stirred reactor. Combustion and Flame 2017;185:4-15.
534 [37] Cai L, Sudholt A, Lee DJ, Egolfopoulos FN, Pitsch H, Westbrook CK, et al. Chemical kinetic
535 study of a novel lignocellulosic biofuel: Di-n-butyl ether oxidation in a laminar flow reactor and
536 flames. Combustion and Flame 2014;161(3):798-809.
537 [38] Jacobs S, Döntgen M, Alquaity ABS, Kopp WA, Kröger LC, Burke U, et al. Detailed kinetic
538 modeling of dimethoxymethane. Part II: Experimental and theoretical study of the kinetics and
539 reaction mechanism. Combustion and Flame 2019;205:522-33.
540 [39] Vermeire FH, Carstensen H-H, Herbinet O, Battin-Leclerc F, Marin GB, Van Geem KM.
541 Experimental and modeling study of the pyrolysis and combustion of dimethoxymethane.
542 Combustion and Flame 2018;190:270-83.
543 [40] Cai L, Jacobs S, Langer R, vom Lehn F, Heufer KA, Pitsch H. Auto-ignition of oxymethylene
544 ethers (OMEn, n = 2–4) as promising synthetic e-fuels from renewable electricity: shock tube
545 experiments and automatic mechanism generation. Fuel 2020;264.
546 [41] Li R, Herreros JM, Tsolakis A, Yang W. Chemical kinetic study on ignition and flame
547 characteristic of polyoxymethylene dimethyl ether 3 (PODE3). Fuel 2020;279.
548 [42] He T, Wang Z, You X, Liu H, Wang Y, Li X, et al. A chemical kinetic mechanism for the low- and

549 intermediate-temperature combustion of Polyoxymethylene Dimethyl Ether 3 (PODE 3). Fuel
550 2018;212:223-35.
551 [43] Sun W, Wang G, Li S, Zhang R, Yang B, Yang J, et al. Speciation and the laminar burning
552 velocities of poly(oxymethylene) dimethyl ether 3 (POMDME 3) flames: An experimental and
553 modeling study. Proceedings of the Combustion Institute 2017;36(1):1269-78.
554 [44] Zhou C-W, Li Y, Burke U, Banyon C, Somers KP, Ding S, et al. An experimental and chemical
555 kinetic modeling study of 1,3-butadiene combustion: Ignition delay time and laminar flame speed
556 measurements. Combustion and Flame 2018;197:423-38.
557 [45] Li Y, Zhou C-W, Somers KP, Zhang K, Curran HJ. The oxidation of 2-butene: A high pressure
558 ignition delay, kinetic modeling study and reactivity comparison with isobutene and 1-butene.
559 Proceedings of the Combustion Institute 2017;36(1):403-11.
560 [46] NIST Chemistry WebBook.https://webbook.nist.gov/chemistry/.
561 [47] PubChem. National Institutes of Health:https://pubchem.ncbi.nlm.nih.gov/.
562 [48] ChemSpider. Royal Society of Chemistry:http://www.chemspider.com/.
563 [49] The 8th internaltional conference: Fuel Science-From Production to Propulsion.
564 2020:https://www.fuelcenter.rwth-aachen.de/global/show_document.asp?id=aaaaaaaaaqayulb.
565 [50] Benson SW. Thermochemical kinetics: methods for the estimation of thermochemical data and
566 rate parameters. 2nd ed. New York: John Wiley & Sons; 1976.
567 [51] Lay TH, Bozzelli JW, Dean AM, Ritter ER. Hydrogen Atom Bond Increments for Calculation of
568 Thermodynamic Properties of Hydrocarbon Radical Species. The Journal of Physical Chemistry
569 1995;99(39):14514-27.
570 [52] Glaude PA, Pitz WJ, Thomson MJ. Chemical kinetic modeling of dimethyl carbonate in an

opposed-flow diffusion flame. Proceedings of the Combustion Institute 2005;30(1):1111-8.

[53] Tee LS, Gotoh S, Stewart WE. Molecular Parameters for Normal Fluids. Lennard-Jones 12-6 Potential. Industrial & Engineering Chemistry Fundamentals 1966;5(3):356-63.

[54] Yaws CL. Yaws' handbook of thermodynamic and physical properties of chemical compounds : physical, thermodynamic and transport properties for 5,000 organic chemical compounds. Knovel; 2003.

[55] AP1700 Material property calculation and inquiry platform.http://www.ap1700.com/.

[56] Gauthier BM, Davidson DF, Hanson RK. Shock tube determination of ignition delay times in full-blend and surrogate fuel mixtures. Combustion and Flame 2004;139(4):300-11.

[57] Heufer KA, Olivier H. Determination of ignition delay times of different hydrocarbons in a new high pressure shock tube. Shock Waves 2010;20(4):307-16.

AUTHOR INFORMATION

Corresponding Author

*E-mail: a.tsolakis@bham.ac.uk

ORCID

Runzhao Li: 0000-0001-5120-9849

Jose Martin Herreros: 0000-0002-6939-121X

Athanasios Tsolakis: 0000-0002-6222-6393

Notes

The authors declare no competing financial interest.